

**Nonlinear Wave Propagation and Solitary Wave
Formation in Two-Dimensional Heterogeneous Media**

Thesis by

Manuel Quezada de Luna, B.Sc.

In Partial Fulfillment of the Requirements For the Degree of
Masters of Science

King Abdullah University of Science and Technology,
Thuwal, Kingdom of Saudi Arabia

May, 2011

The thesis of Manuel Quezada de Luna is approved by the examination committee.

Committee Chairperson:

David I. Ketcheson

Committee member:

Aslan Kasimov

Committee member:

George Turkiyyah

ABSTRACT

Nonlinear Wave Propagation and Solitary Wave Formation
 in Two-Dimensional Heterogeneous Media
 Manuel Quezada de Luna

Solitary wave formation is a well studied nonlinear phenomenon arising in propagation of dispersive nonlinear waves under suitable conditions. In non-homogeneous materials, dispersion may happen due to effective reflections between the material interfaces. This dispersion has been used along with nonlinearities to find solitary wave formation using the one-dimensional p-system. These solitary waves are called stegotons.

The main goal in this work is to find two-dimensional stegoton formation. To do so we consider the nonlinear two-dimensional p-system with variable coefficients and solve it using finite volume methods.

The second goal is to obtain effective equations that describe the macroscopic behavior of the variable coefficient system by a constant coefficient one. This is done through a homogenization process based on multiple-scale asymptotic expansions. We compare the solution of the effective equations with the finite volume results and find a good agreement. Finally, we study some stability properties of the homogenized equations and find they and one-dimensional versions of them are unstable in general.

ACKNOWLEDGMENTS

I would like to sincerely thank my supervisor David I. Ketcheson for his continuous guidance and encouragement throughout the course of this work. His enthusiasm and valuable feedback for research made my study very enjoyable and exciting and ultimately fruitful with rich experience. I would also like to thank him for providing me with an amazing research environment.

I thank the members of my committee David Ketcheson, Aslan Kasimov and George Turkiyyah for all their valuable feedback, which helped me improve some of the results presented in this work.

I also would like to thank all PetClaw team for their continuous support, specifically to Amal Alghamdi, David Ketcheson, Aron Ahmadia and Matteo Parsani.

I thank my parents for their continuous encouragement and my siblings for bearing with me for my negligence towards them during this journey and their deep moral support at all times.

Lastly, I would like to thank the people at KAUST, Thuwal, Makkah Province, Saudi Arabia for providing support and resources for this research work.

TABLE OF CONTENTS

Signature Approvals	2
Abstract	3
Acknowledgments	4
Introduction	9
Summary	11
I Background	13
I Finite volume methods	15
I.1 The Riemann problem	15
I.1.1 Linear case	16
I.1.2 Nonlinear case	18
I.2 Approximate Riemann solvers	19
I.3 Finite volume methods	20
I.4 Godunov-type methods	22
I.4.1 First order accurate	22
I.4.2 Higher order accuracy	22
I.5 F-wave finite volume approach	23

I.6 Finite volume methods for 2D systems	24
I.6.1 Dimensional splitting	25
I.6.2 Unsplit methods	25
II Homogenization	27
II 2D stegotons	29
III 1D p-system	31
III.1 System of equations	31
III.2 Conservative vs. non-conservative approach	32
III.2.1 Non-conservative method	33
III.2.2 Conservative method	34
III.2.3 Numerical results	35
III.3 1D stegoton formation	35
IV 2D p-system	37
IV.1 Domain	37
IV.2 Systems of equations	38
IV.3 Riemann solvers	39
IV.3.1 Riemann solver in x-direction	40
IV.3.2 Riemann solver in y-direction	42
IV.3.3 Riemann solver for the transverse corrections	43
IV.3.3.1 Correction to the vertical fluctuations	43
IV.3.3.2 Correction to the horizontal fluctuations	44
IV.4 Dimensional splitting vs. Flux differencing with transverse corrections	45
IV.5 2D stegoton formation	46
IV.5.1 Importance of numerical dissipation	47
IV.5.2 2D Stegotons	49

IV.5.2.1	Checkerboard domain	49
IV.5.2.2	Heterogeneity in a single direction	51
IV.5.3	Stegotons on 2D rectangular domains	52
IV.6	Convergence study	54
III	Homogenization	58
V	Derivation of homogenized equations	61
V.1	Inverted system for the fluxes	61
V.2	Asymptotic expansion	63
V.3	Terms of $O(\delta^{-1})$	65
V.4	Terms of $O(1)$	66
V.4.1	Averaged $O(1)$ system	67
V.4.2	Ansatz for $O(1)$ system	67
V.5	Terms of $O(\delta)$	70
V.5.1	Averaged $O(\delta)$ system	71
V.5.2	Ansatz for $O(\delta)$ system	72
V.6	Terms of $O(\delta^2)$	77
V.6.1	Averaged $O(\delta^2)$ system	78
V.7	Specific problem	80
V.7.1	Combining the homogenized systems	82
VI	Numerical solution of the homogenized system	84
VI.1	Spatial discretization	84
VI.2	Time integration	85
VI.3	Linear case	86
VI.4	Nonlinear case	87

VIIAbout the stability of the homogenized system	92
VII.1Stability of 1D homogenized system	95
VII.2Another unstable 1D homogenized system	98
Conclusions	101

INTRODUCTION

In 1965, Zabusky and Kruskal [1] “observed unusual nonlinear interaction among ‘solitary-wave pulses’ propagating in nonlinear dispersive media” considering the Korteweg-deVries equation:

$$u_t + uu_x + \delta^2 u_{xxx} = 0, \quad (.0.1)$$

which, among others, models the long wave behavior of shallow water waves. By considering a small δ^2 , they observed that initially the solution in (.0.1) is dominated by the first two terms making the solution behave as the Burgers equation; i.e., a smooth initial profile steepens whenever the slope is negative, tending to shock formation. As a consequence, the third derivative of u becomes important introducing oscillations behind the wave front due to dispersion effects. These oscillations grow leading to the break up of the initial profile into a finite number of solitary wave pulses, which they called solitons. The key ingredients for this phenomenon are nonlinearity to steepen the initial profile and dispersion to break it up into solitary waves.

It has been found [2, 3, 4, 5] that hyperbolic systems in heterogeneous media may present dispersion effects even without explicit dispersion terms. The heterogeneity creates reflections at the interfaces leading effectively to dispersion. In 2003, LeVeque and Yong [5] considered a nonlinear system of hyperbolic equations (without dispersion terms) to describe elastic wave propagation in a 1D heterogeneous medium and found that an initial profile splits into solitary waves, which they called stegotons.

In the present work, we consider nonlinear wave propagation in 2D heterogeneous media modeled by a system of variable-coefficient partial differential equations (PDEs) without dispersion terms. The main goal is to find 2D solitary wave formation. Following [5], the problem is tackled in two different ways, numerically and through homogenization. Numerically, the system is solved under different circumstances using finite volume methods implemented in Clawpack [6] and PetClaw [7]. Clawpack is a hyperbolic solver based on Riemann solvers while PetClaw is a parallelization of Clawpack based on PETSc [8]. In addition, effective equations are obtained using a homogenization technique based on multiple scale asymptotic expansions. Different approaches to perform the homogenization may be considered, in this work we extend the ideas in [3] to the 2D scenario. These effective equations are then solved using a pseudospectral discretization in space and an implicit integration in time. Finally, both solutions are compared.

From the finite volume solutions we find solitary wave formation, extending the results in [5] to 2D. For the homogenized system, we find a good agreement between its numerical solution and the numerical solution of the variable-coefficient system through finite volumes. The homogenized equations we find are, however, not stable in general. Trying to understand the nature and source of such instability we study the 1D version following the same homogenized approach and find the 1D homogenized system is also unstable in general. Finally, we considered the work in [5] where a different homogenization procedure is performed for the same 1D system and find those equations are unstable in general as well.

SUMMARY

In this work, we mainly look to answer whether stegotons may or may not exist in 2D. In addition, we try to get an effective system from a nonlinear wave propagation model in 2D heterogeneous media through a homogenization process.

As mentioned in the introduction, stegotons were found and presented as solitary waves formed by the propagation of 1D nonlinear waves in heterogeneous media. In this work, we study numerically the 2D situation finding that stegotons may exist in 2D as well. In addition, we present simulations for different scenarios in 2D.

The wave propagation in heterogeneous media may be modeled, and is modeled in this work, by fast variable coefficient PDEs. To solve numerically these equations, one must use a grid finer than the structure of the heterogeneity, which increases the computational cost. The homogenized equations have constant coefficients; as a result, one may use coarser grids. In addition, having homogenized equations may help to understand specific behavior of the system, which would be hard to understand through the numerical solution. We derive homogenized equations and compare them with the solution of the variable-coefficient system through finite volumes having a good agreement. The homogenized equations we derived are, however, not stable in general while the variable coefficient system is stable. Trying to understand the source of the instability, we consider the 1D case through two different homogenization approaches and find they are unstable in general as well.

This work is divided in three parts. The first part presents some background

split into two chapters. Chapter I is devoted to finite volume methods and topics such as Riemann problems, approximate Riemann solvers, finite volume methods, Godunov-type methods, f-wave finite volume approach and finite volume methods for 2D systems are introduced. In Chapter II, the main ideas of homogenization are presented.

In the second part, we mainly present the results regarding 2D stegoton formation considering the p-system. In this part, we consider in Chapter III the 1D situation, compare a conservative and a non-conservative method and reproduce the results in [5] regarding 1D stegotons. Afterwards, the 2D system is considered in Chapter IV. To do so, we first introduce the 2D p-system and all Riemann solvers used during the finite volume simulations and compare two finite volume approaches for 2D. Finally, all results showing solitary wave formation in 2D heterogeneous media are shown.

The third part is devoted to finding and solving homogenized equations for a different system. Here we first find the homogenized system, solve it numerically, and make some comments regarding its stability.

Finally, some conclusions and future research are discussed.

Part I

Background

In this part we introduce the background required for the remaining parts of this work. Two chapters are included one devoted to important aspects of finite volume methods and another to the main homogenization ideas.

Chapter I

Finite volume methods

In this section the main ideas of finite volume methods are presented. The topics covered are the Riemann problem, approximate Riemann solvers, finite volume methods, Godunov-type methods, f-wave finite volume approach, and finite volume methods in 2D. Most of the material in this section is reviewed from [9] and in less proportion in [10, 11].

I.1 The Riemann problem

The implementation of finite volume methods in Clawpack is based on the solution of a Riemann problem at each grid cell interface. In this section, the Riemann problem is presented.

The Riemann problem consists of a hyperbolic equation (or system of them):

$$\bar{q}_t + \bar{f}(\bar{q})_x = \bar{0}, \quad (\text{I.1.1})$$

along with initial discontinuous data:

$$\bar{q}(x, 0) = \begin{cases} \bar{q}_l, & \forall x < 0, \\ \bar{q}_r, & \forall x > 0, \end{cases}$$

where \bar{q} is the solution vector, $\bar{f}(\bar{q})$ is the flux and \bar{q}_l and \bar{q}_r are the left and right states of the discontinuous initial condition. We use a bar above the variables to denote vectors.

I.1.1 Linear case

From (I.1.1), assuming $\bar{f}(\bar{q})$ is linear and using the chain rule, we get:

$$\bar{q}_t + \mathbf{A}\bar{q}_x = \bar{0},$$

where $\mathbf{A} \in \mathbb{R}^{m,m} = \mathbf{f}'(\bar{q})$ is the Jacobian matrix of the flux $\bar{f}(\bar{q})$. Decompose \mathbf{A} using an eigenvalue decomposition to obtain:

$$\bar{q}_t + \mathbf{R}\Lambda\mathbf{R}^{-1}\bar{q}_x = \bar{0}, \quad (\text{I.1.2})$$

where \mathbf{R} is the eigenvector matrix and Λ is the corresponding diagonal eigenvalue matrix whose entries are $\lambda^1 \leq \lambda^2 \leq \dots \leq \lambda^p \leq \dots \leq \lambda^m$. Multiply (I.1.2) from the left by \mathbf{R}^{-1} to get:

$$\bar{w}_t + \Lambda\bar{w}_x = \bar{0}, \quad (\text{I.1.3})$$

where $\bar{w} = \mathbf{R}^{-1}\bar{q}$ is the vector of characteristic variables. Equation (I.1.3) is a system of decoupled advection equations with initial data given by:

$$\bar{w}(x, 0) = \mathbf{R}^{-1}\bar{q}(x, 0).$$

Each of these advection equations can be solved exactly. The solution of w^p , the

p_{th} characteristic variable, is given by:

$$w^p(x, t) = \begin{cases} w_l^p, & \forall (x - \lambda^p t) < 0, \\ w_r^p, & \forall (x - \lambda^p t) > 0. \end{cases}$$

Once the solution for \bar{w} is computed, one can obtain $\bar{q}(x, t)$ by:

$$\bar{q} = \mathbf{R}\bar{w}.$$

We see that the solution $\bar{q}(x, t)$ is made of a superposition of m waves. At a given point in the x-t plane, w^p will be either w_r^p or w_l^p depending on whether $x - \lambda^p t$ is positive or negative. Therefore, the solution $\bar{q}(x, t)$ can be constructed by:

$$\bar{q}(x, t) = \sum_{p:(x-\lambda^p t)<0} w_l^p \bar{r}^p + \sum_{p:(x-\lambda^p t)>0} w_r^p \bar{r}^p.$$

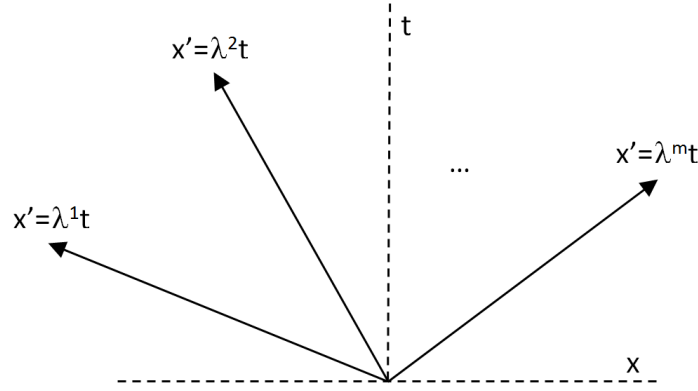


Figure I.1.1: x-t plane showing m characteristics.

If one plots $(x - \lambda^p t) = 0$ in the x-t plane for $\forall p = 1, \dots, m$, one would obtain a plot like the one showed in figure I.1.1. We obtain wedges split by the characteristics, $x = \lambda^1 t, x = \lambda^2 t, \dots, x = \lambda^p t, \dots, x = \lambda^m t$. Note that for all points within a given wedge, the p_{th} wave carries the same information. Therefore, the solution within a given wedge is constant. In addition, note that whenever we enter a new wedge, just one characteristic is carrying new information. As a result, there will be a jump in

$\bar{q}(x, t)$ given by a jump in a single simple wave w . By definition, the jump in the p_{th} simple wave is given by:

$$(w_r^p - w_l^p) \bar{r}^p \equiv \alpha^p \bar{r}^p,$$

which means that the jump in $\bar{q}(x, t)$ from one wedge to another is proportional to an eigenvector of \mathbf{A} . Following this idea, the jump in $\bar{q}(x, t)$ is decomposed using the eigenvectors of \mathbf{A} as follows:

$$\Delta \bar{q} = \bar{q}_r - \bar{q}_l = \sum_{p=1}^m \alpha^p \bar{r}^p = \sum_{p=1}^m \bar{\mathcal{W}}^p = \mathbf{R} \bar{\alpha},$$

where α 's are the coefficients of the expansion and $\bar{\mathcal{W}}^p$ is a wave that denotes the jump in q across the p -th wave. Hence, these waves can be used to compute \bar{q} knowing either \bar{q}_l or \bar{q}_r by:

$$\begin{aligned} \bar{q} &= \bar{q}_l + \sum_{p:x-\lambda^p t > 0} \bar{\mathcal{W}}^p, \\ \bar{q} &= \bar{q}_r + \sum_{p:x-\lambda^p t < 0} \bar{\mathcal{W}}^p. \end{aligned}$$

I.1.2 Nonlinear case

There are different approaches to solve nonlinear hyperbolic equations using finite volume methods. Two possible approaches are to solve the Riemann problem exactly or to find a local linearization at every point of the domain and then proceed as in the linear case. Even considering a local linearization, one can proceed in different ways such as decomposing the jump in the solution using the eigenvectors of the linearized flux Jacobian or decomposing the jump in the flux using the same eigenvectors.

In this work, we consider a linearized version of the flux Jacobian at every point of the domain instead of solving the Riemann problem exactly. Afterwards, we consider

the case of decomposing the jump in the solution and later decomposing the jump in the flux.

I.2 Approximate Riemann solvers

Consider the discretized domain $[x_{i-1}, x_{i+1}]$ to solve the conservation law:

$$\bar{q}_t + \bar{f}(\bar{q})_x = \bar{q}_t + \mathbf{f}'(\bar{q})\bar{q}_x = \bar{0}. \quad (\text{I.2.1})$$

Consider $\hat{\mathbf{A}}_{i-\frac{1}{2}}$ to be a valid linear approximation of the flux Jacobian near the data \bar{Q}_{i-1} and \bar{Q}_i ; i.e., $\hat{\mathbf{A}}_{i-\frac{1}{2}} \approx \mathbf{f}'(\bar{q})$. Doing so, (I.2.1) becomes:

$$\bar{q}_t + \hat{\mathbf{A}}_{i-\frac{1}{2}}\bar{q}_x = \bar{0}. \quad (\text{I.2.2})$$

In order for (I.2.2) to be hyperbolic, we need $\hat{\mathbf{A}}_{i-\frac{1}{2}}$ to be diagonalizable with real eigenvalues. In addition, for (I.2.2) to be consistent with (I.2.1), we require $\hat{\mathbf{A}}_{i-\frac{1}{2}} \rightarrow \mathbf{f}'(\bar{q})$ as the grid is refined. Once the linearization is found, one proceeds as in the linear case to solve the approximate Riemann problem.

A difficulty may arise if one picks the linearization without mimicking the conservative nature of the hyperbolic system and shock waves are present. In this situation, the Rankine-Hugoniot conditions are not satisfied and, consequently, the shock speed would not be correct. In order for the approximate Riemann solver to be conservative, we must have:

$$\hat{\mathbf{A}}_{i-\frac{1}{2}}(\bar{Q}_i - \bar{Q}_{i-1}) = \bar{f}_i(\bar{Q}_i) - \bar{f}_{i-1}(\bar{Q}_{i-1}), \quad (\text{I.2.3})$$

which comes from the fact that if $\hat{\mathbf{A}}_{i-\frac{1}{2}}\bar{q} = \bar{f}(\bar{q})$, then (I.2.2) is in conservation form. Recall the Rankine-Hugoniot conditions given by:

$$s(\bar{Q}_i - \bar{Q}_{i-1}) = \bar{f}_i(\bar{Q}_i) - \bar{f}_{i-1}(\bar{Q}_{i-1}). \quad (\text{I.2.4})$$

Plug (I.2.4) into (I.2.3) to get:

$$\hat{\mathbf{A}}_{i-\frac{1}{2}}(\bar{Q}_i - \bar{Q}_{i-1}) = s(\bar{Q}_i - \bar{Q}_{i-1}),$$

which is an eigenvalue problem. Hence, $(\bar{Q}_i - \bar{Q}_{i-1})$ is an eigenvector of $\hat{\mathbf{A}}_{i-\frac{1}{2}}$ and s , the shock speed, is the corresponding eigenvalue.

I.3 Finite volume methods

Consider a hyperbolic equation:

$$q_t + f(q) = 0,$$

where q is a conserved quantity (or a vector of conserved quantities) and $f(q)$ is the flux of q . This conservation law can be written in integral form as:

$$\frac{d}{dt} \int_a^b q(x, t) dx = -[f(q(b, t)) - f(q(a, t))], \quad (\text{I.3.1})$$

where a and b are the beginning and the end of the domain considered. Consider now a discretized domain where $C_i = [x_{i-\frac{1}{2}}, x_{i+\frac{1}{2}}]$ represents the i_{th} grid cell. Considering $x \in C_i$, equation (I.3.1) becomes:

$$\frac{d}{dt} \int_{C_i} q(x, t) dx = -[f(q(x_{i+\frac{1}{2}}, t)) - f(q(x_{i-\frac{1}{2}}, t))], \forall x \in [x_{i-\frac{1}{2}}, x_{i+\frac{1}{2}}], \quad (\text{I.3.2})$$

Now, using the fundamental theorem of calculus, we integrate (I.3.2) in time from t_n , the current time, to t_{n+1} , the next time step, to obtain:

$$\begin{aligned} \frac{1}{\Delta x} \int_{C_i} q(x, t_{n+1}) dx &= \frac{1}{\Delta x} \int_{C_i} q(x, t_n) dx \\ &\quad - \frac{\Delta t}{\Delta x} \left[\frac{1}{\Delta t} \int_{t_n}^{t_{n+1}} f(q(x_{i+\frac{1}{2}}, t)) dt - \frac{1}{\Delta t} \int_{t_n}^{t_{n+1}} f(q(x_{i-\frac{1}{2}}, t)) dt \right]. \end{aligned} \quad (\text{I.3.3})$$

Let Q_i^n denote the cell average:

$$Q_i^n \approx \frac{1}{\Delta x} \int_{C_i} q(x, t_n) dx. \quad (\text{I.3.4})$$

Similarly, let $F_{i-\frac{1}{2}}^n$ denote the time flux integral:

$$F_{i-\frac{1}{2}}^n \approx \frac{1}{\Delta t} \int_{t_n}^{t_{n+1}} f(q(x_{i-\frac{1}{2}}, t)) dt. \quad (\text{I.3.5})$$

Using (I.3.4) and (I.3.5) equation (I.3.3) becomes:

$$Q_i^{n+1} = Q_i^n - \frac{\Delta t}{\Delta x} \left[F_{i+\frac{1}{2}}^n - F_{i-\frac{1}{2}}^n \right]. \quad (\text{I.3.6})$$

Since the function q is not known, the time integral of the flux must be approximated in somehow. Considering that in hyperbolic equations the information propagates with finite speeds, $\int_{t_n}^{t_{n+1}} f(q(x_{i-\frac{1}{2}}, t)) dt$ is approximated using Q_{i-1}^n and Q_i^n . Let $\mathcal{F}(Q_{i-1}^n, Q_i^n)$ denote this approximation. Doing so, (I.3.6) becomes:

$$Q_i^{n+1} = Q_i^n - \frac{\Delta t}{\Delta x} [\mathcal{F}(Q_i^n, Q_{i+1}^n) - \mathcal{F}(Q_{i-1}^n, Q_i^n)], \quad (\text{I.3.7})$$

which is the basic finite volume discretization. Depending on a specific form of $\mathcal{F}(Q_{i-1}^n, Q_i^n)$, we have different methods.

I.4 Godunov-type methods

I.4.1 First order accurate

Godunov-type methods consists in the following three steps:

1. Reconstruction. Approximate the cell average $\frac{1}{\Delta x} \int_{C_i} q(x, t_n) dx$ using a polynomial $\tilde{q}^n(x, t_n)$. If a constant polynomial is considered, then $\tilde{q}^n(x, t_n) = Q_i^n$, which corresponds to Godunov's method.
2. Evolve the hyperbolic equation using as initial data $\tilde{q}^n(x_n, t_n)$ to get $\tilde{q}^n(x_n, t_{n+1})$.
3. Average $\tilde{q}^n(x_n, t_{n+1})$ to get:

$$Q_i^{n+1} \approx \frac{1}{\Delta x} \int_{C_i} \tilde{q}^n(x, t_{n+1}) dx,$$

which is the average solution at the next time.

If we consider a constant polynomial reconstruction, the evolution of $\tilde{q}^n(x_n, t_n)$ in step 2 is obtained by a Riemann problem. Doing this, we obtain a Riemann problem at each grid interface. If the time step is small enough, the waves coming from different Riemann problems will not interact with each other. Let $q^*(Q_{i-1}^n, Q_i^n)$ denote the state at $x_{i-\frac{1}{2}}$. The time flux integral is then:

$$F_{i-\frac{1}{2}}^n \approx \frac{1}{\Delta t} \int_{t_n}^{t_{n+1}} f(q^*(Q_{i-1}^n, Q_i^n)) dt \equiv \mathcal{F}(Q_{i-1}^n, Q_i^n). \quad (\text{I.4.1})$$

Plugging (I.4.1) into (I.3.7) completes the finite volume Godunov type methods.

I.4.2 Higher order accuracy

If one wants to obtain more than first order accuracy, one has to use better than constant reconstruction. Several options for the reconstruction are available. A common approach is to use a linear reconstruction. To do so, one has to choose a slope for the linear reconstruction. Different options for the slope yield different algorithms. This

may create oscillations near discontinuities, which can be avoided by using slope limiters. These methods limit the magnitude of the slope near the discontinuity so that oscillations are avoided. Again different slope limiters will give different methods.

I.5 F-wave finite volume approach

This method, proposed in [11], consists in decomposing the jump in the flux using the eigenvectors of some linearization of the flux Jacobian.

Consider the conservation law:

$$\bar{q}_t + \bar{f}(\bar{q})_x = \bar{0},$$

which can be viewed as:

$$\bar{q}_t + \mathbf{f}'(\bar{q})\bar{q}_x = \bar{0}.$$

Using a local linearization of the flux Jacobian such that $\hat{\mathbf{A}}_{i-\frac{1}{2}} \in \mathbb{R}^{m,m} \approx \mathbf{f}'(\bar{q})$, we obtain:

$$\bar{q}_t + \hat{\mathbf{A}}_{i-\frac{1}{2}}\bar{q}_x = \bar{0}.$$

The eigenvectors of $\hat{\mathbf{A}}_{i-\frac{1}{2}}$ are used to expand the jump in the flux so that:

$$\begin{aligned}\Delta \bar{F}_{i-\frac{1}{2}} &= \beta_{i-\frac{1}{2}}^1 \bar{r}_{i-\frac{1}{2}}^1 + \cdots + \beta_{i-\frac{1}{2}}^p \bar{r}_{i-\frac{1}{2}}^p + \dots, \\ &= \bar{\mathcal{Z}}_{i-\frac{1}{2}}^1 + \cdots + \bar{\mathcal{Z}}_{i-\frac{1}{2}}^p + \cdots + \bar{\mathcal{Z}}_{i-\frac{1}{2}}^m, \\ &= \mathbf{R}_{i-\frac{1}{2}} \bar{\beta}_{i-\frac{1}{2}},\end{aligned}$$

where β' s are the coefficients of the expansion, \bar{r}' s are the eigenvectors of $\hat{\mathbf{A}}_{i-\frac{1}{2}}$, \mathbf{R}

is the corresponding eigenvector matrix and $\bar{\mathcal{Z}}_{i-\frac{1}{2}}^p$ is the p_{th} f-wave whose speed s^p is given by the corresponding p_{th} eigenvalue of $\hat{\mathbf{A}}_{i-\frac{1}{2}}$:

$$s_{i-\frac{1}{2}}^p = \lambda_{i-\frac{1}{2}}^p.$$

One can compute $\bar{\beta}_{i-\frac{1}{2}}$ by:

$$\bar{\beta}_{i-\frac{1}{2}} = \mathbf{R}_{i-\frac{1}{2}}^{-1} \Delta \bar{F}_{i-\frac{1}{2}}.$$

Finally, the right and left going fluctuations, which are quantities that consider the net effect of all right and left going waves respectively [9, 10], are given by:

$$\begin{aligned}\mathcal{A}^+ \Delta \bar{Q}_{i-\frac{1}{2}} &= \sum_{p: s_{i-\frac{1}{2}}^p > 0} \bar{\mathcal{Z}}_{i-\frac{1}{2}}^p, \\ \mathcal{A}^- \Delta \bar{Q}_{i-\frac{1}{2}} &= \sum_{p: s_{i-\frac{1}{2}}^p < 0} \bar{\mathcal{Z}}_{i-\frac{1}{2}}^p.\end{aligned}$$

Two main advantages of the f-wave approach are particularly convenient for this work:

- The method is conservative, which is important since the considered system is nonlinear.
- The method is easily applicable to heterogeneous media when no change in the eigenvalue is present in the whole domain and the flux is continuous. These two conditions are true for the problems in this work.

I.6 Finite volume methods for 2D systems

In this section, some approaches to solve 2D problems are introduced.

I.6.1 Dimensional splitting

In this approach the multidimensional problem is split into 1D problems. Given a 2D problem as:

$$\bar{q}_t + \mathbf{A}\bar{q}_x + \mathbf{B}\bar{q}_y = \bar{0},$$

one would obtain:

$$\bar{q}_t + \mathbf{A}\bar{q}_x = \bar{0},$$

$$\bar{q}_t + \mathbf{B}\bar{q}_y = \bar{0}.$$

Afterwards, finite volume methods for 1D problems are applied to solve sequentially first for the x direction and then for the y direction. Within Clawpack, two time splitting methods are available: Godunov splitting and Strang splitting. Using Godunov splitting gives:

$$\begin{aligned}\bar{Q}_{ij}^* &= \bar{Q}_{ij}^n - \frac{\Delta t}{\Delta x} \left(\bar{F}_{i+\frac{1}{2},j}^n - \bar{F}_{i-\frac{1}{2},j}^n \right), \\ \bar{Q}_{ij}^{n+1} &= \bar{Q}_{ij}^* - \frac{\Delta t}{\Delta y} \left(\bar{G}_{i,j+\frac{1}{2}}^* - \bar{G}_{i,j-\frac{1}{2}}^* \right),\end{aligned}$$

where \bar{F}^n is a numerical flux in x and \bar{G}^* represents a numerical flux in y after applying the algorithm for the x direction. Choosing different numerical fluxes \bar{F}^n and \bar{G}^* gives different methods.

I.6.2 Unsplit methods

This approach consists of a discretization in time as well as a discretization in space.

Consider a 2D hyperbolic equation in conservation form:

$$\bar{q}_t + \bar{f}(\bar{q})_x + \bar{g}(\bar{q})_y = \bar{0},$$

where $\bar{f}(\bar{q})$ and $\bar{g}(\bar{q})$ are fluxes in x and y respectively. Discretizing in space and time, one obtains:

$$\bar{Q}_{ij}^{n+1} = \bar{Q}_{ij}^n - \frac{\Delta t}{\Delta x} \left[\bar{F}_{i+\frac{1}{2},j}^n - \bar{F}_{i-\frac{1}{2},j}^n \right] - \frac{\Delta t}{\Delta y} \left[\bar{G}_{i,j+\frac{1}{2}}^n - \bar{G}_{i,j-\frac{1}{2}}^n \right],$$

where \bar{F}^n and \bar{G}^n are numerical fluxes. By choosing these numerical fluxes in different ways, one obtains different methods such as the Lax-Wendroff method, Godunov's method, and others. As in the case of 1D, second order methods can be obtained by using linear reconstruction and applying slope limiters. In Clawpack, this method is implemented by solving 1D Riemann problems at each cell interface and computing the influence of the flux at the given interface to the corresponding transverse interfaces.

Chapter II

Homogenization

This section presents a brief review of the key ideas behind homogenization based on multiple scale asymptotic expansion. A detailed explanation of homogenization can be found in [12, 13] and for understanding on asymptotic expansion one may refer to [14, 15]. Homogenization has been widely used in different areas to study composite materials; some examples can be found in [13, 16, 17, 18, 19, 2, 4, 5, 3]. In the context of hyperbolic equations, it has been found that the heterogeneity leads to dispersion effects captured at high order corrections [2, 3, 4, 5, 20].

Homogenization can be applied on problems where different scales are present by averaging over the small scales. By doing so, we lose local information in such scales and recover their effect only on the macroscopic scales.

Through multiple scale asymptotic expansion, one obtains a leading order system and some corrections to it. Afterwards, homogenization is obtained by averaging such systems over the microscopic scales. In this work, we introduce small scales in space. As a result, the average is obtained using the operator:

$$\langle \cdot \rangle = \int_0^1 \int_0^1 (\cdot) d\hat{x} d\hat{y}, \quad (\text{II.0.1})$$

where \hat{x} and \hat{y} represent small scales in space. To obtain the homogenized systems

the following two assumptions are essential:

- The non-averaged solution is continuous with respect to the small scales.
- The averaged solution is independent of the small scales.

Specific steps may vary between different approaches. In this work we follow closely [3] and extend this approach to a 2D situation. Two main steps are applied to the systems coming from the multiple scale asymptotic expansion. First, the averaging operator is used to get a homogenized system. Then, an ansatz for the non-averaged solution is proposed looking to get ODEs that define them once we plug them into the current system. The second step is required if further corrections are needed. Finally, all systems are combined based on the original expansion and a final average is applied.

Part II

2D stegotons

The present section is mainly devoted to the solution of the 2D p-system in non-linear heterogeneous media using finite volumes. As mentioned in the introduction, the objective is to find solitary wave formation where the dispersion comes from the heterogeneity.

The section is divided into two chapters, one for the 1D and another for the 2D problem. The 1D case is studied and presented due to its importance in the solution of the 2D system by dimensional splitting or flux differencing with transverse corrections. Within the 1D chapter, the system is solved using a conservative and a non-conservative approach and results comparing both methods are presented. In addition, results from [5] showing 1D stegoton formation are reproduced.

In Chapter IV, the 2D p-system is solved using the conservative method with dimensional splitting and flux differencing with transverse corrections. The corresponding Riemann solvers are presented as well as results comparing both approaches. Afterwards, results obtained regarding 2D stegoton formation are shown as well as a convergence study.

Chapter III

1D p-system

In this chapter, the system to consider is first introduced. A conservative and a non-conservative approach are then considered to solve the system and results comparing them are shown. Finally, results from [5] about 1D stegoton formation are reproduced.

III.1 System of equations

The 1D p-system in terms of elasticity is given by:

$$\epsilon_t - u_x = 0, \quad (\text{III.1.1a})$$

$$\rho(x) u_t - \sigma(\epsilon)_x = 0, \quad (\text{III.1.1b})$$

where $\epsilon(x, t)$ is the strain, $\sigma(\epsilon)$ is the stress, $u(x, t)$ is the velocity and $\rho(x)$ is the density. The system can also be viewed as a conservation law:

$$\bar{q}_t + \bar{f}(\bar{q})_x = \bar{0},$$

where $\bar{q} = \begin{bmatrix} \epsilon \\ \hat{u} \end{bmatrix}$ is the solution and $\bar{f}(\bar{q}) = \begin{bmatrix} -\rho^{-1}\hat{u} \\ -\sigma(\epsilon) \end{bmatrix}$ is the flux with $\hat{u} = \rho u$ denoting the momentum in x . Considering the system in its conservation form is convenient for the finite volume implementation. The system is closed by introducing a constitutive relation for $\sigma = \sigma(\epsilon)$. Following [5], we choose:

$$\sigma(\epsilon) = \exp(E(x)\epsilon) - 1,$$

where E is the Young modulus.

III.2 Conservative vs. non-conservative approach

To solve (III.1.1), we consider an approximate Riemann solver so that:

$$\bar{q}_t + \hat{\mathbf{A}}_{i-\frac{1}{2}} \bar{q}_x = \bar{0},$$

where $\hat{\mathbf{A}}_{i-\frac{1}{2}}$ is a local linearization of the flux Jacobian $\mathbf{f}'(\bar{q})$ and the subscript $i - \frac{1}{2}$ denotes the interface between cells $i - 1$ and i . Indeed, what we need for the finite volume implementation are just the corresponding eigenvalues and eigenvectors. The approximated flux Jacobian $\hat{\mathbf{A}}_{i-\frac{1}{2}}$ has one negative and one positive eigenvalue and neither changes sign. Therefore, there will be one wave w^1 propagating to the left and other w^2 to the right. Since the medium is nonlinear and heterogeneous, we use ρ_{i-1} , E_{i-1} and ϵ_{i-1} to obtain \bar{r}^1 and λ^1 , the left eigenvector and its corresponding eigenvalue. Similarly, \bar{r}^2 and λ^2 are computed considering ρ_i , E_i and ϵ_i . Note that for this to be valid, we must assure during the implementation that the material interfaces coincide with the grid interfaces. Based on [21], the eigenvectors of $\hat{\mathbf{A}}_{i-\frac{1}{2}}$ are:

$$\begin{aligned}\bar{r}_{i-\frac{1}{2}}^1 &= \begin{bmatrix} 1 \\ \sqrt{\rho_{i-1}\sigma_{\epsilon,i-1}} \end{bmatrix}, \\ \bar{r}_{i-\frac{1}{2}}^2 &= \begin{bmatrix} 1 \\ -\sqrt{\rho_i\sigma_{\epsilon,i}} \end{bmatrix},\end{aligned}$$

and the corresponding eigenvalues are:

$$\begin{aligned}\lambda_{i-\frac{1}{2}}^1 &= -\sqrt{\frac{\sigma_{\epsilon,i-1}}{\rho_{i-1}}}, \\ \lambda_{i-\frac{1}{2}}^2 &= \sqrt{\frac{\sigma_{\epsilon,i}}{\rho_i}}.\end{aligned}$$

III.2.1 Non-conservative method

The non-conservative approach we consider is based on decomposing the jump in the solution in terms of waves proportional to the eigenvectors of the linearized Jacobian. Doing so, we obtain:

$$\begin{aligned}\Delta\bar{Q}_{i-\frac{1}{2}} &= \alpha_{i-\frac{1}{2}}^1 \bar{r}_{i-\frac{1}{2}}^1 + \alpha_{i-\frac{1}{2}}^2 \bar{r}_{i-\frac{1}{2}}^2, \\ &= \bar{\mathcal{W}}_{i-\frac{1}{2}}^1 + \bar{\mathcal{W}}_{i-\frac{1}{2}}^2,\end{aligned}$$

where $\bar{\mathcal{W}}_{i-\frac{1}{2}}^p$ is the p_{th} wave and α 's are the coefficients of the expansion and are computed by:

$$\bar{\alpha} = \mathbf{R}^{-1} \Delta\bar{Q}_{i-\frac{1}{2}},$$

where \mathbf{R} is the matrix of eigenvectors.

The speed $s_{i-\frac{1}{2}}^p$ of the wave $\bar{\mathcal{W}}_{i-\frac{1}{2}}^p$ is given by the p_{th} eigenvalue $\lambda_{i-\frac{1}{2}}^p$. Finally, the fluctuations are:

$$\begin{aligned}\mathcal{A}^- \Delta \bar{Q}_{i-\frac{1}{2}} &= s_{i-\frac{1}{2}}^1 \bar{\mathcal{W}}_{i-\frac{1}{2}}^1, \\ \mathcal{A}^+ \Delta \bar{Q}_{i-\frac{1}{2}} &= s_{i-\frac{1}{2}}^2 \bar{\mathcal{W}}_{i-\frac{1}{2}}^2.\end{aligned}$$

III.2.2 Conservative method

The conservative method we consider is based on the f-wave approach [11]. In this method, the jump in the flux is decomposed using the eigenvectors of the linearized flux Jacobian. Doing so, we get:

$$\begin{aligned}\Delta \bar{F}_{i-\frac{1}{2}} &= \beta_{i-\frac{1}{2}}^1 \bar{r}_{i-\frac{1}{2}}^1 + \beta_{i-\frac{1}{2}}^2 \bar{r}_{i-\frac{1}{2}}^2, \\ &= \bar{\mathcal{Z}}_{i-\frac{1}{2}}^1 + \bar{\mathcal{Z}}_{i-\frac{1}{2}}^2,\end{aligned}$$

where $\bar{\mathcal{Z}}_{i-\frac{1}{2}}^p$ is the p_{th} wave and β' s are the coefficients of the expansion and are computed by:

$$\bar{\beta} = \mathbf{R}^{-1} \Delta \bar{F}_{i-\frac{1}{2}},$$

The speed $s_{i-\frac{1}{2}}^p$ of the wave $\bar{\mathcal{Z}}_{i-\frac{1}{2}}^p$ is again given by the p_{th} eigenvalue $\lambda_{i-\frac{1}{2}}^p$. Finally, the fluctuations are:

$$\begin{aligned}\mathcal{A}^- \Delta \bar{Q}_{i-\frac{1}{2}} &= \bar{\mathcal{Z}}_{i-\frac{1}{2}}^1, \\ \mathcal{A}^+ \Delta \bar{Q}_{i-\frac{1}{2}} &= \bar{\mathcal{Z}}_{i-\frac{1}{2}}^2.\end{aligned}$$

III.2.3 Numerical results

To compare the conservative and the non-conservative methods we consider a homogeneous medium with:

$$\rho = E = 1. \quad (\text{III.2.1})$$

Figure III.2.1 shows the strain for different times using both methods with periodic boundary conditions. We can see the solutions seem to match whenever no shocks are present. At the moment shocks start to occur, a disagreement in the solutions starts to happen. This is because the non-conservative method is not satisfying the Rankine Hugoniot conditions and, therefore, the shock speed is not correct.

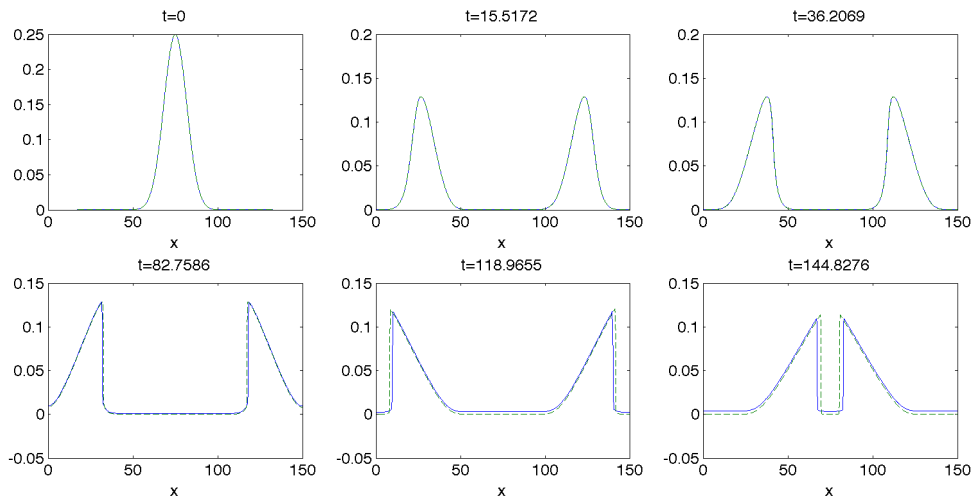


Figure III.2.1: Solution for 1D nonlinear system (III.1.1) for a homogeneous medium with material properties given by (III.2.1) using a conservative (dashed line) and a nonconservative (solid line) method.

III.3 1D stegoton formation

Using the conservative method, we reproduce the results in [5] regarding stegoton formation. For these simulations we consider:

$$\rho_1 = E_1 = 1, \quad (\text{III.3.1a})$$

$$\rho_2 = E_2 = 4. \quad (\text{III.3.1b})$$

Figure III.3.1 shows the stegotons for the strain and the stress.

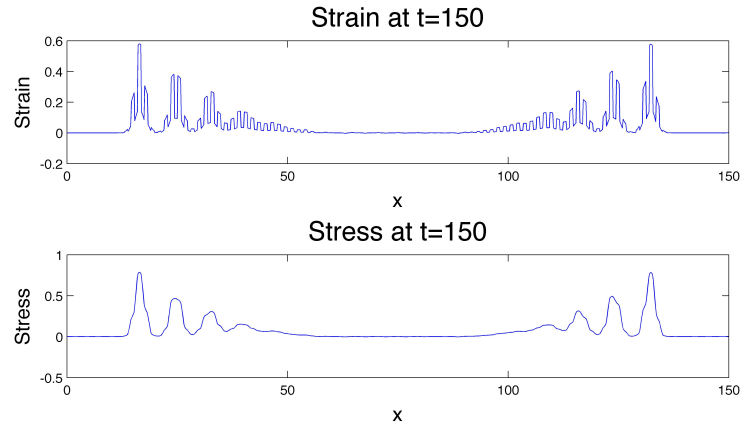


Figure III.3.1: Solution for 1D nonlinear system (III.1.1) for a heterogeneous medium with material properties given by (III.3.1). Stegotons in 1D are formed for the strain (top) and stress (bottom)

Chapter IV

2D p-system

In the current chapter, we first introduce the p-system in 2D. The system is then solved using dimensional splitting and flux differencing. To do so, the corresponding approximate Riemann solvers are presented. Afterwards, results comparing both methods are shown. Finally, the results obtained regarding 2D stegotons are shown.

IV.1 Domain

The domain considered in this part of the work is of a checkerboard type. Figure IV.1.1 shows a characterization of the domain.

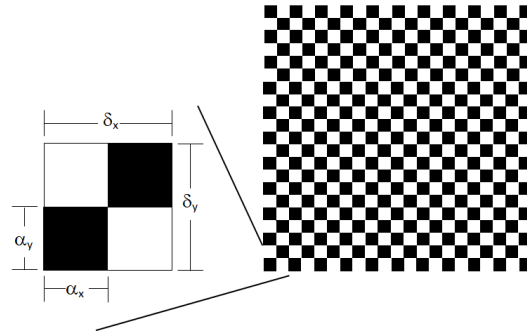


Figure IV.1.1: Checkerboard domain.

IV.2 Systems of equations

We can think of this system as a particular simplified model that describes propagation of elastic waves. In a solid, an elastic wave is composed of longitudinal or P-waves and transversal or S-waves [9]. If we neglect the S-waves and assume the stress is the same in all directions, the propagation of elastic waves can be modeled by:

$$\epsilon_t - \nabla \cdot \bar{u} = 0, \quad (\text{IV.2.1a})$$

$$\rho(\bar{x}) \bar{u}_t - \nabla \sigma(\epsilon, \bar{x}) = 0, \quad (\text{IV.2.1b})$$

where ϵ represents the strain, $\bar{u} = [u, v]^T$ is the velocity vector, $\rho = \rho(\bar{x})$ is the material density, $\sigma(\epsilon, \bar{x})$ is the stress and $\bar{x} = [x, y]^T$ is the position vector. One can think of system (IV.2.1) as a model describing the propagation of compressive waves in a gas whose properties change in space.

System (IV.2.1) can be written in scalar form:

$$\epsilon_t - u_x - v_y = 0,$$

$$\rho u_t - \sigma_x = 0,$$

$$\rho v_t - \sigma_y = 0,$$

or, equivalently, as a hyperbolic system:

$$\bar{q}_t + \bar{f}(\bar{q}, \bar{x})_x + \bar{g}(\bar{q}, \bar{x})_y = \bar{0}, \quad (\text{IV.2.2})$$

where:

$$\bar{q} = \begin{bmatrix} \epsilon \\ \hat{u} \\ \hat{v} \end{bmatrix}, \quad \bar{f}(\bar{q}, \bar{x}) = \begin{bmatrix} -\rho^{-1}(\bar{x}) \hat{u} \\ -\sigma(\epsilon, \bar{x}) \\ 0 \end{bmatrix}, \quad \bar{g}(\bar{q}, \bar{x}) = \begin{bmatrix} -\rho^{-1}(\bar{x}) \hat{v} \\ 0 \\ -\sigma(\epsilon, \bar{x}) \end{bmatrix},$$

where $\hat{u} = \rho u$ and $\hat{v} = \rho v$ are the momentum in x and y respectively. The vector functions $\bar{f}(\bar{q}, \bar{x})$ and $\bar{g}(\bar{q}, \bar{x})$ are the fluxes in x and y respectively and \bar{q} is the solution vector. Equation (IV.2.2) is in a non-linear conservation form, which is convenient for the finite volume implementation.

IV.3 Riemann solvers

For the dimensional splitting method, we need to have 1D Riemann solvers in each direction. On the other hand, for the flux differencing with transverse corrections we require not just Riemann solvers in each direction, but also transverse corrections for the fluxes at each interface. In this section we present all the Riemann solvers. Refer to section I.6 for a further explanation.

A linearized problem is considered extending the idea presented in [21] for the 1D case to the 2D situation. Doing so, system (IV.2.2) becomes:

$$\bar{q}_t + \hat{\mathbf{A}}_{i-\frac{1}{2},j}\bar{q}_x + \hat{\mathbf{B}}_{i,j-\frac{1}{2}}\bar{q}_y = \bar{0},$$

where $\hat{\mathbf{A}}_{i-\frac{1}{2},j}$ and $\hat{\mathbf{B}}_{i,j-\frac{1}{2}}$ are the linearized flux Jacobians. In both 2D methods we consider, the system is first treated as 1D problems in each direction. As a result, we need to solve sequentially:

$$\begin{aligned}\bar{q}_t + \hat{\mathbf{A}}_{i-\frac{1}{2},j} \bar{q}_x &= \bar{0}, \\ \bar{q}_t + \hat{\mathbf{B}}_{i,j-\frac{1}{2}} \bar{q}_y &= \bar{0},\end{aligned}$$

for the x and y direction respectively.

IV.3.1 Riemann solver in x-direction

This Riemann solver must consider the propagation in x :

$$\bar{q}_t + \hat{\mathbf{A}}_{i-\frac{1}{2},j} \bar{q}_x = \bar{0}.$$

Following the conservative approach for the variable coefficients in 1D we decomposed the jump in the flux as:

$$\begin{aligned}\Delta \bar{F}_{i-\frac{1}{2},j} &= \beta_{i-\frac{1}{2},j}^1 \bar{r}_{i-\frac{1}{2},j}^1 + \beta_{i-\frac{1}{2},j}^2 \bar{r}_{i-\frac{1}{2},j}^2 + \beta_{i-\frac{1}{2},j}^3 \bar{r}_{i-\frac{1}{2},j}^3, \\ &= \bar{\mathcal{Z}}_{i-\frac{1}{2},j}^1 + \bar{\mathcal{Z}}_{i-\frac{1}{2},j}^2 + \bar{\mathcal{Z}}_{i-\frac{1}{2},j}^3,\end{aligned}$$

where the β' s are the coefficients of the expansion and \bar{r}' s are the eigenvectors of $\hat{\mathbf{A}}_{i-\frac{1}{2},j}$ and are given by:

$$\bar{r}_{i-\frac{1}{2},j}^1 = \begin{bmatrix} r_{i-\frac{1}{2},j}^{11} \\ 1 \\ 0 \end{bmatrix}; \quad \bar{r}_{i-\frac{1}{2},j}^2 = \begin{bmatrix} 0 \\ 0 \\ 1 \end{bmatrix}; \quad \bar{r}_{i-\frac{1}{2},j}^3 = \begin{bmatrix} r_{i-\frac{1}{2},j}^{13} \\ 1 \\ 0 \end{bmatrix},$$

where:

$$\begin{aligned} r_{i-\frac{1}{2},j}^{11} &= \frac{1}{\sqrt{\rho_{i-1,j}\sigma_{\epsilon,i-1,j}}}, \\ r_{i-\frac{1}{2},j}^{13} &= \frac{-1}{\sqrt{\rho_{i,j}\sigma_{\epsilon,i,j}}}. \end{aligned}$$

The $\bar{\beta}_{i-\frac{1}{2},j}$ vector is computed by:

$$\bar{\beta}_{i-\frac{1}{2},j} = \mathbf{R}_{i-\frac{1}{2},j}^{-1} \Delta \bar{F}_{i-\frac{1}{2},j},$$

where $\mathbf{R}_{i-\frac{1}{2},j}$ is the matrix of eigenvectors.

The speed $s_{i-\frac{1}{2},j}^p$ of the wave $\bar{\mathcal{Z}}_{i-\frac{1}{2},j}^p$ is given by the p_{th} eigenvalue $\lambda_{i-\frac{1}{2},j}^p$, which are:

$$\begin{aligned} \lambda_{i-\frac{1}{2},j}^1 &= s_{i-\frac{1}{2},j}^1 = -\sqrt{\frac{\sigma_{\epsilon,i-1,j}}{\rho_{i-1,j}}}, \\ \lambda_{i-\frac{1}{2},j}^2 &= s_{i-\frac{1}{2},j}^2 = 0 \\ \lambda_{i-\frac{1}{2},j}^3 &= s_{i-\frac{1}{2},j}^3 = \sqrt{\frac{\sigma_{\epsilon,i,j}}{\rho_{i,j}}}. \end{aligned}$$

Finally, the fluctuations are:

$$\begin{aligned} \mathcal{A}^- \Delta \bar{Q}_{i-\frac{1}{2},j} &= \bar{\mathcal{Z}}_{i-\frac{1}{2},j}^1, \\ \mathcal{A}^+ \Delta \bar{Q}_{i-\frac{1}{2},j} &= \bar{\mathcal{Z}}_{i-\frac{1}{2},j}^3. \end{aligned}$$

Note that just two f-waves appear in the fluctuations; i.e., the standing wave $\bar{\mathcal{Z}}_{i-\frac{1}{2},j}^2$ will have no influence in the updating of the solution.

IV.3.2 Riemann solver in y-direction

This Riemann solver must consider the propagation in y:

$$\bar{q}_t + \hat{\mathbf{B}}_{i,j-\frac{1}{2}} \bar{q}_y = \bar{0}.$$

Using the conservative f-wave method, we decompose the jump in the flux as:

$$\begin{aligned}\Delta \bar{F}_{i,j-\frac{1}{2}} &= \beta_{i,j-\frac{1}{2}}^1 \bar{r}_{i,j-\frac{1}{2}}^1 + \beta_{i,j-\frac{1}{2}}^2 \bar{r}_{i,j-\frac{1}{2}}^2 + \beta_{i,j-\frac{1}{2}}^3 \bar{r}_{i,j-\frac{1}{2}}^3, \\ &= \bar{\mathcal{Z}}_{i,j-\frac{1}{2}}^1 + \bar{\mathcal{Z}}_{i,j-\frac{1}{2}}^2 + \bar{\mathcal{Z}}_{i,j-\frac{1}{2}}^3,\end{aligned}$$

where the β' s are the coefficients of the expansion and \bar{r}' s are the eigenvectors of $\hat{\mathbf{B}}_{i,j-\frac{1}{2}}$ and are given by:

$$\bar{r}_{i,j-\frac{1}{2}}^1 = \begin{bmatrix} r_{i,j-\frac{1}{2}}^{11} \\ 0 \\ 1 \end{bmatrix}; \quad \bar{r}_{i,j-\frac{1}{2}}^2 = \begin{bmatrix} 0 \\ 1 \\ 0 \end{bmatrix}; \quad \bar{r}_{i,j-\frac{1}{2}}^3 = \begin{bmatrix} r_{i,j-\frac{1}{2}}^{13} \\ 0 \\ 1 \end{bmatrix}, \quad (\text{IV.3.1})$$

where:

$$\begin{aligned}r_{i,j-\frac{1}{2}}^{11} &= \frac{1}{\sqrt{\rho_{i,j-1} \sigma_{\epsilon,i,j-1}}}, \\ r_{i,j-\frac{1}{2}}^{13} &= \frac{-1}{\sqrt{\rho_{i,j} \sigma_{\epsilon,i,j}}}.\end{aligned}$$

The $\bar{\beta}_{i,j-\frac{1}{2}}$ vector is computed by:

$$\bar{\beta}_{i,j-\frac{1}{2}} = \mathbf{R}_{i,j-\frac{1}{2}}^{-1} \Delta \bar{F}_{i,j-\frac{1}{2}}.$$

The speed $s_{i,j-\frac{1}{2}}^p$ of the wave $\bar{\mathcal{Z}}_{i,j-\frac{1}{2}}^p$ is given by the p_{th} eigenvalue $\lambda_{i,j-\frac{1}{2}}^p$, which are:

$$\lambda_{i,j-\frac{1}{2}}^1 = s_{i,j-\frac{1}{2}}^1 = -\sqrt{\frac{\sigma_{\epsilon,i,j-1}}{\rho_{i,j-1}}}, \quad (\text{IV.3.2a})$$

$$\lambda_{i,j-\frac{1}{2}}^2 = s_{i,j-\frac{1}{2}}^2 = 0 \quad (\text{IV.3.2b})$$

$$\lambda_{i,j-\frac{1}{2}}^3 = s_{i,j-\frac{1}{2}}^3 = \sqrt{\frac{\sigma_{\epsilon,i,j}}{\rho_{i,j}}}. \quad (\text{IV.3.2c})$$

Finally, the fluctuations are:

$$\mathcal{B}^- \Delta \bar{Q}_{i,j-\frac{1}{2}} = \bar{\mathcal{Z}}_{i,j-\frac{1}{2}}^1,$$

$$\mathcal{B}^+ \Delta \bar{Q}_{i,j-\frac{1}{2}} = \bar{\mathcal{Z}}_{i,j-\frac{1}{2}}^3.$$

Again just two waves contribute in the updating of the solution.

IV.3.3 Riemann solver for the transverse corrections

In Clawpack, the unsplit method is implemented through a transverse Riemann solver that decomposes the horizontal going fluctuations into up and down going corrections and the vertical fluctuations into right and left going corrections. In this section, we present these transverse Riemann solvers.

IV.3.3.1 Correction to the vertical fluctuations

To correct the vertical fluctuations, the horizontal ones are decomposed into up and down going fluctuations using the eigenvectors of $\hat{\mathbf{B}}_{i,j-\frac{1}{2}}$ from (IV.3.1):

$$\mathcal{A}^\pm \Delta \bar{Q}_{i-\frac{1}{2},j} = \gamma_{i,j-\frac{1}{2}}^1 \bar{r}_{i,j-\frac{1}{2}}^1 + \gamma_{i,j-\frac{1}{2}}^2 \bar{r}_{i,j-\frac{1}{2}}^2 + \gamma_{i,j-\frac{1}{2}}^3 \bar{r}_{i,j-\frac{1}{2}}^3,$$

where the superscript \pm denotes the right and left directions and γ 's are the coefficients of the expansion, which are computed by:

$$\bar{\gamma}_{i,j-\frac{1}{2}} = \mathbf{R}_{i,j-\frac{1}{2}}^{-1} \mathcal{A}^\pm \Delta \bar{Q}_{i-\frac{1}{2},j},$$

where \mathbf{R} is the matrix of corresponding eigenvectors of \mathbf{B} .

The speed of the waves in the vertical direction determines the amount of horizontal fluctuation that must be added to the vertical one. These speeds are given by the eigenvalues of $\hat{\mathbf{B}}_{i,j-\frac{1}{2}}$ from (IV.3.2). Finally, the corrections to the vertical fluctuations are:

$$\mathcal{B}^- \mathcal{A}^\pm \Delta \bar{Q}_{i-\frac{1}{2},j} = s_{i,j-\frac{1}{2}}^1 \gamma_{i,j-\frac{1}{2}}^1 \bar{r}_{i,j-\frac{1}{2}}^1, \quad (\text{IV.3.3a})$$

$$\mathcal{B}^+ \mathcal{A}^\pm \Delta \bar{Q}_{i-\frac{1}{2},j} = s_{i,j-\frac{1}{2}}^3 \gamma_{i,j-\frac{1}{2}}^3 \bar{r}_{i,j-\frac{1}{2}}^3. \quad (\text{IV.3.3b})$$

IV.3.3.2 Correction to the horizontal fluctuations

The corrections to the horizontal fluctuations are obtained in an analogous way. Those corrections are:

$$\mathcal{A}^- \mathcal{B}^\pm \Delta \bar{Q}_{i,j-\frac{1}{2}} = s_{i-\frac{1}{2},j}^1 \gamma_{i-\frac{1}{2},j}^1 \bar{r}_{i-\frac{1}{2},j}^1, \quad (\text{IV.3.4a})$$

$$\mathcal{A}^+ \mathcal{B}^\pm \Delta \bar{Q}_{i,j-\frac{1}{2}} = s_{i-\frac{1}{2},j}^3 \gamma_{i-\frac{1}{2},j}^3 \bar{r}_{i-\frac{1}{2},j}^3, \quad (\text{IV.3.4b})$$

where we use the eigenvalues and eigenvectors of $\hat{\mathbf{A}}_{i-\frac{1}{2},j}$ instead.

IV.4 Dimensional splitting vs. Flux differencing with transverse corrections

In this section we compare numerical results of (IV.2.1) using dimensional splitting and flux differencing with transverse corrections where the corrections are given by (IV.3.3) and (IV.3.4). This is intended to see qualitative differences between those approaches. Figure IV.4.1 shows the corresponding results considering 100 grid cells in each direction, a linear constitutive relation given by $\sigma = E\epsilon$ and the following parameters:

$$E_1 = \rho_1 = 1, \quad (\text{IV.4.1a})$$

$$E_2 = \rho_2 = 10, \quad (\text{IV.4.1b})$$

$$\delta_x = \delta_y = 1, \quad (\text{IV.4.1c})$$

$$\alpha_x = \alpha_y = 0.5. \quad (\text{IV.4.1d})$$

The initial condition is given by a 2D Gaussian pulse centered at the origin with amplitude of 10 and variance in x and y of 0.1. The boundary conditions are of reflecting type.

Although we don't know the exact solution, we know it must be symmetric. Considering this, it is evident the better quality of the flux differencing method using the computed corrections against dimensional splitting.

For the simulations in this section Clawpack was used instead of PetClaw. This is possible since the domain and the number of grid cells is small enough to handle the computations on a serial computer. For the long simulations, even though the

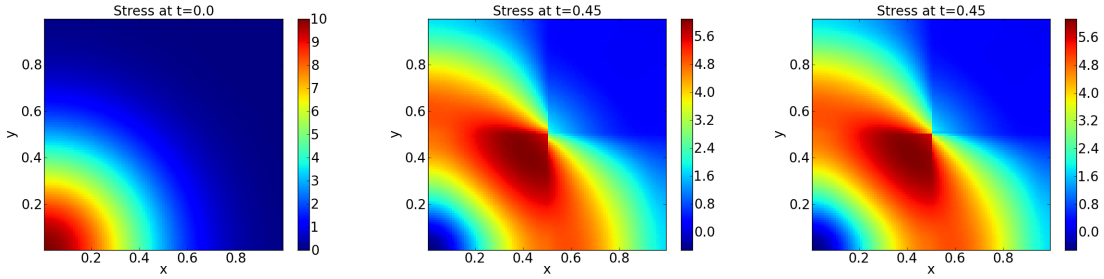


Figure IV.4.1: Solution for (IV.2.1) with parameters given by (IV.4.1). Shown is the initial condition (left), solution with dimensional splitting (middle) and with flux differencing with transverse corrections (right). The better quality by applying transverse corrections may be noticed by the more symmetric solution.

quality is better with flux differencing methods, we use dimensional splitting since at the moment this is the only available option in PetClaw.

IV.5 2D stegoton formation

In the current section, we present all results related with 2D stegoton formation for the system (IV.2.1). For all simulations in the remaining of this chapter we use the same initial condition, which is a 2D Gaussian pulse with amplitude of 10 and variance in x and y of 5. In addition, we use a nonlinear constitutive relation given by:

$$\sigma = \exp(E\epsilon) - 1.$$

Finally, unless otherwise indicated, we consider:

$$\delta_x = \delta_y = 1,$$

$$\alpha_x = \alpha_y = 0.5.$$

IV.5.1 Importance of numerical dissipation

The numerical solution using finite volume methods has some numerical dissipation that deteriorates the quality of the solution. Increasing the number of grid points diminishes this issue. The amount of dissipation introduced by finite volume methods depends on the smoothness of the solution. Having a rapidly varying solution or a discontinuity introduces more dissipation.

Having small numerical dissipation plays an important role in the problem of finding stegoton formation. In 1D this may not be a big problem since the computational cost of increasing the number of grid points per unit of the domain to the point for which numerical dissipation is not an issue anymore is easily affordable. Nevertheless, in 2D this is not the case. As a result, in this work we use PetClaw to run the 2D long simulations on a supercomputer. PetClaw is a PETSc and Clawpack based software to solve hyperbolic partial differential equations on supercomputers.

In the current section, we show simulations of (IV.2.1) that demonstrate the importance of having small numerical dissipation to get stegoton formation.

Considering the following material parameters:

$$E_1 = \rho_1 = 1, \quad (\text{IV.5.1a})$$

$$E_2 = \rho_2 = 5. \quad (\text{IV.5.1b})$$

we obtained simulations using different number of grid cells per unit of the domain. The results are shown in figure IV.5.1. In this case, we use reflecting boundary conditions and place the initial condition at the origin of the domain. We can observe how the dissipation decreases as the number of grid cells increases. When $\text{Ng} = 20$, where Ng is the number of grid cells per unit of the domain, one can hardly observe signs of solitary wave formation. However, for $\text{Ng} = 120$ it is evident that the initial

profile has broken up into different waves.

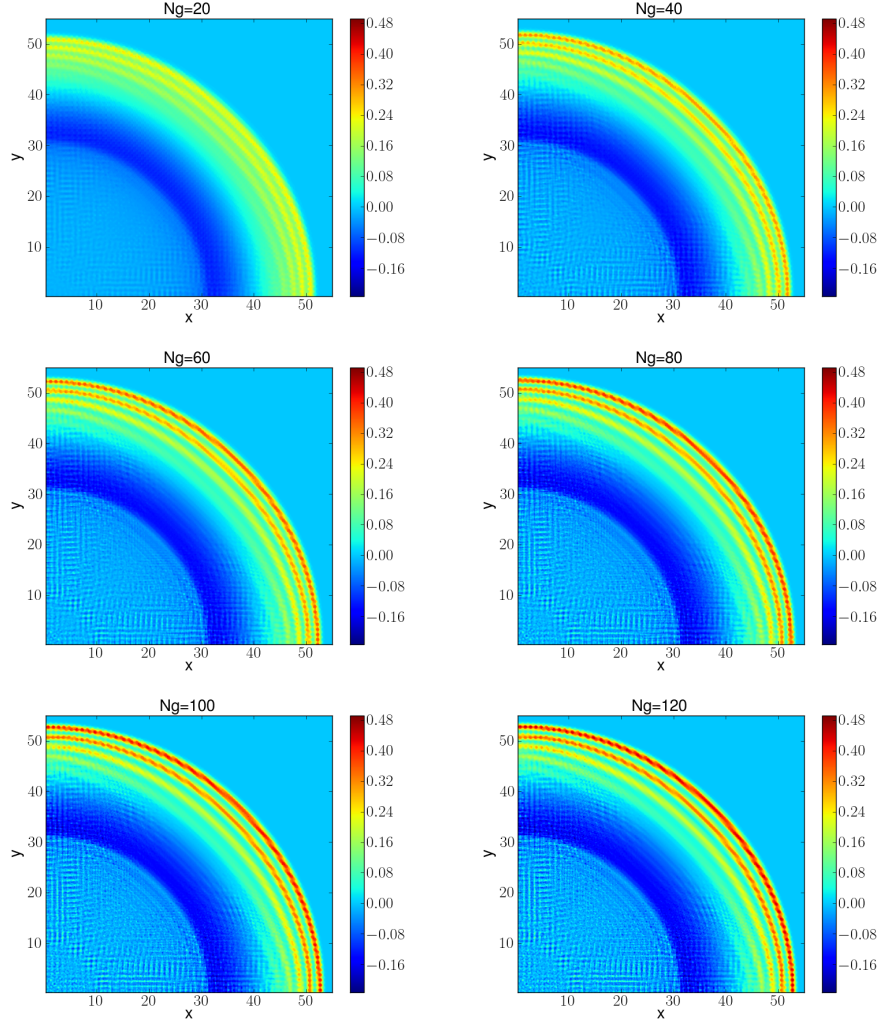


Figure IV.5.1: Stress at $t = 50$ with material parameters given by (IV.5.1) for different number of grid points.

Similarly, in figure IV.5.2 we show the results considering different number of grid points and the following parameters:

$$E_1 = \rho_1 = 1, \quad (\text{IV.5.2a})$$

$$E_2 = \rho_2 = 10. \quad (\text{IV.5.2b})$$

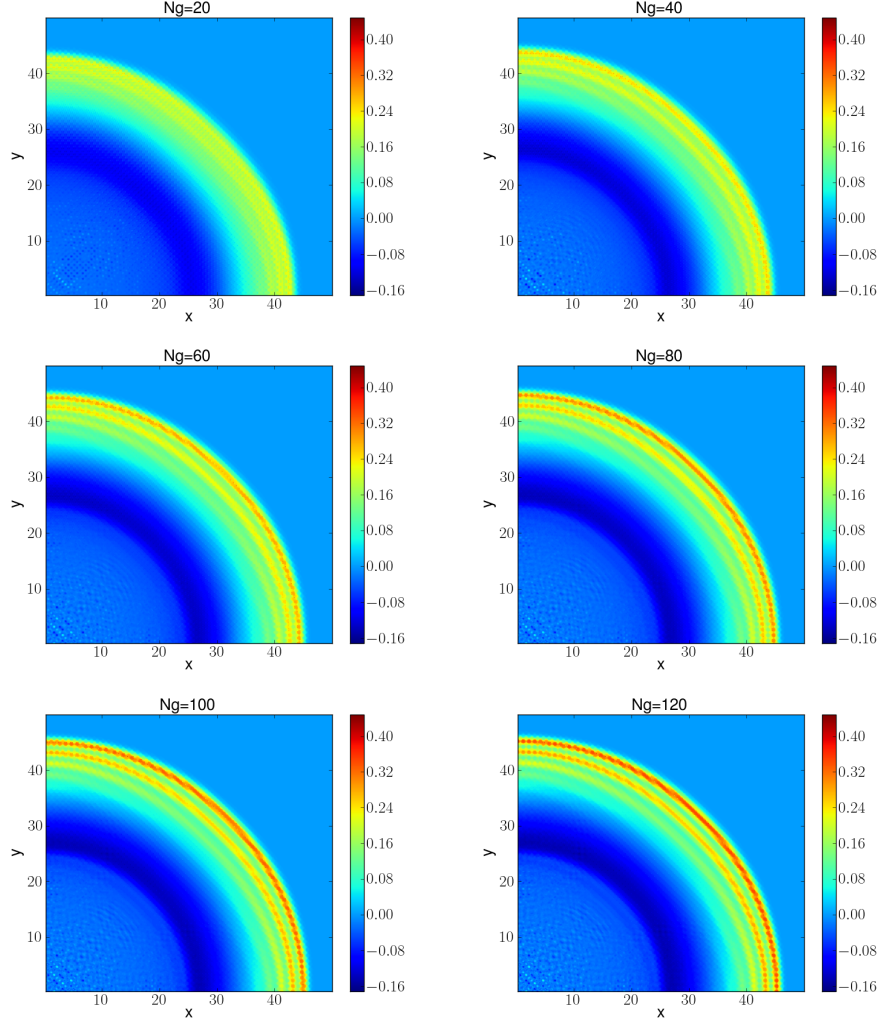


Figure IV.5.2: Stress at $t = 50$ with material parameters given by (IV.5.2) for different number of grid points.

IV.5.2 2D Stegotos

In this section we consider two different scenarios, one with a checkerboard pattern and another with the heterogeneity in just one direction. In both cases, we found solitary wave formation.

IV.5.2.1 Checkerboard domain

Figure IV.5.3 shows results for the stress at $t = 50$ considering a checkerboard domain for two situations, one with:

$$E_1 = \rho_1 = 1, \quad (\text{IV.5.3a})$$

$$E_2 = \rho_2 = 5. \quad (\text{IV.5.3b})$$

and another with:

$$E_1 = \rho_1 = 1, \quad (\text{IV.5.4a})$$

$$E_2 = \rho_2 = 10. \quad (\text{IV.5.4b})$$

In both cases, we implement reflecting boundary conditions and use $\text{Ng} = 120$; i.e., 120 grid cells are considered per unit of the domain. From both scenarios we get 2D solitary wave formation.

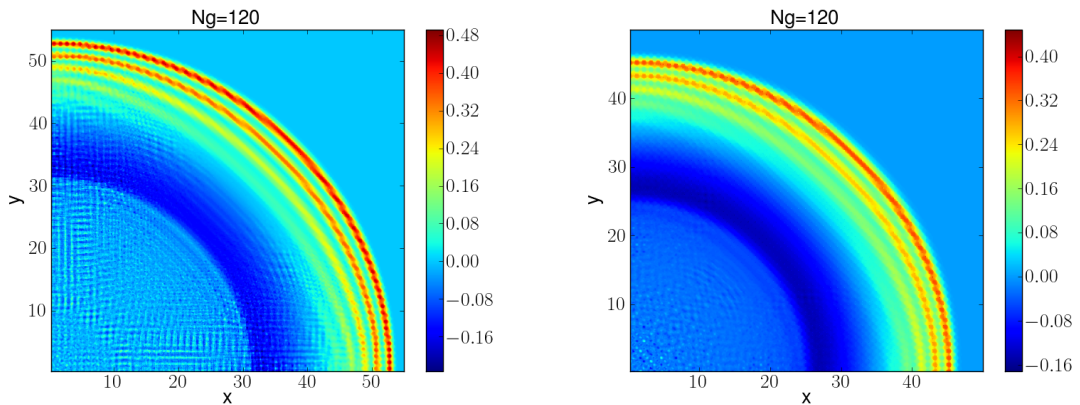


Figure IV.5.3: Stress at $t = 50$ showing 2D solitary wave formation with material parameters given by (IV.5.3) (left) and (IV.5.4) (right). We consider $\text{Ng}=120$ grid cells per unit of the domain.

Considering the parameters given by (IV.5.3), we show in figure IV.5.4 slices of the stress at $t = 50$ at 0° and 45° with respect to the center of the domain. Finally, through a series of snapshots, we show in figure IV.5.5 and IV.5.6 the evolution of the stress and strain respectively from the initial conditions up to $t = 50$ using $\text{Ng}=120$,

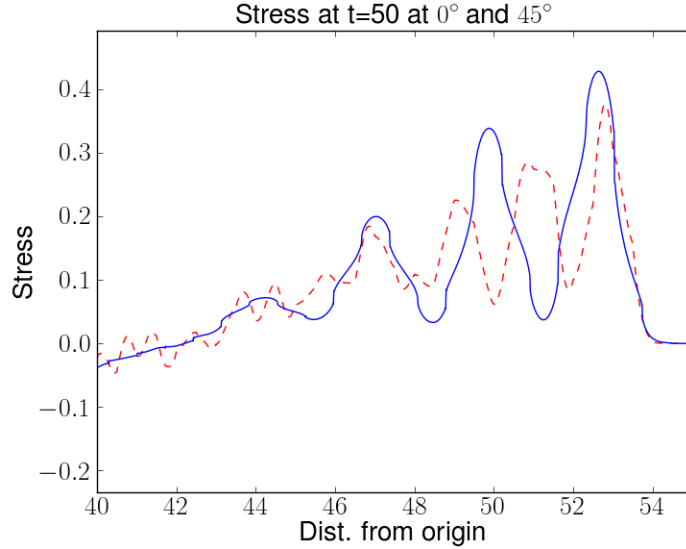


Figure IV.5.4: Slices of the stress at $t = 50$ at 0° (dashed line) and 45° (solid line) with material parameters given by (IV.5.3).

reflecting boundary conditions and the material parameters given by (IV.5.3). As in the 1D situation (see figure III.3.1), the stress, which is one of the fluxes in the conservation law, is continuous. On the other hand, the strain, which is one of the conserve quantities in the conservation law, is discontinuous revealing the heterogeneous structure. From the solution of either the stress or the strain, we can notice the formation of solitary waves.

IV.5.2.2 Heterogeneity in a single direction

In this case we consider a domain heterogeneous in a single direction. Figure IV.5.7 shows the stress at time $t = 50$ when the heterogeneity is just in x using $Ng=120$ and the following material properties:

$$E_1 = \rho_1 = 1, \quad (\text{IV.5.5a})$$

$$E_2 = \rho_2 = 5. \quad (\text{IV.5.5b})$$

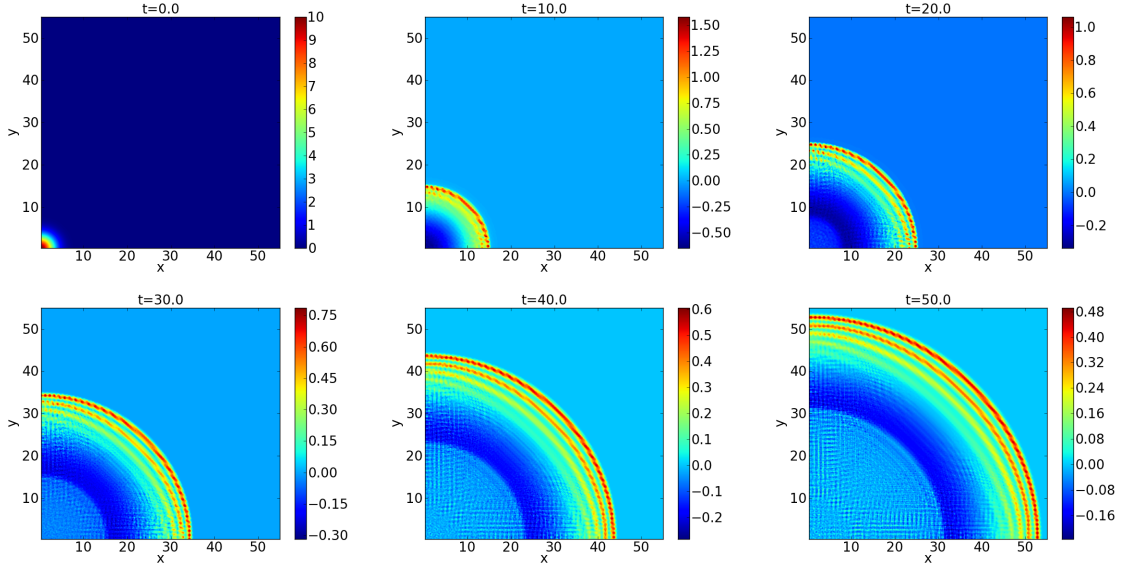


Figure IV.5.5: Evolution of stress with material parameters given by (IV.5.3). We consider $\text{Ng}=120$ grid cells per unit of the domain.

The solitary waves studied in this work are formed by the action of the nonlinear effect, that tends to create shocks, and dispersion coming from effective reflections at the interfaces. In the simulations in this section, we let the material be non-homogeneous just in one direction. As a result, we observe the initial profile breaks up into different waves in the heterogeneous direction while tending to converge to a shock in the homogeneous direction. In addition, we can see that since there is no reflection in the homogeneous direction, the wave travels faster in this direction than in the heterogeneous one. In these simulations absorbing wall boundary conditions are implemented using zeroth-order extrapolation.

IV.5.3 Stegotons on 2D rectangular domains

In [22] a 2D heterogeneous medium is considered for the solution of the p-system. In that work a long thin domain heterogeneous just in x is considered. We consider similar domains but heterogeneous both in x and y . Figure IV.5.8 shows the initial condition and the stress at $t = 50$ for different heterogeneity patterns in y , which

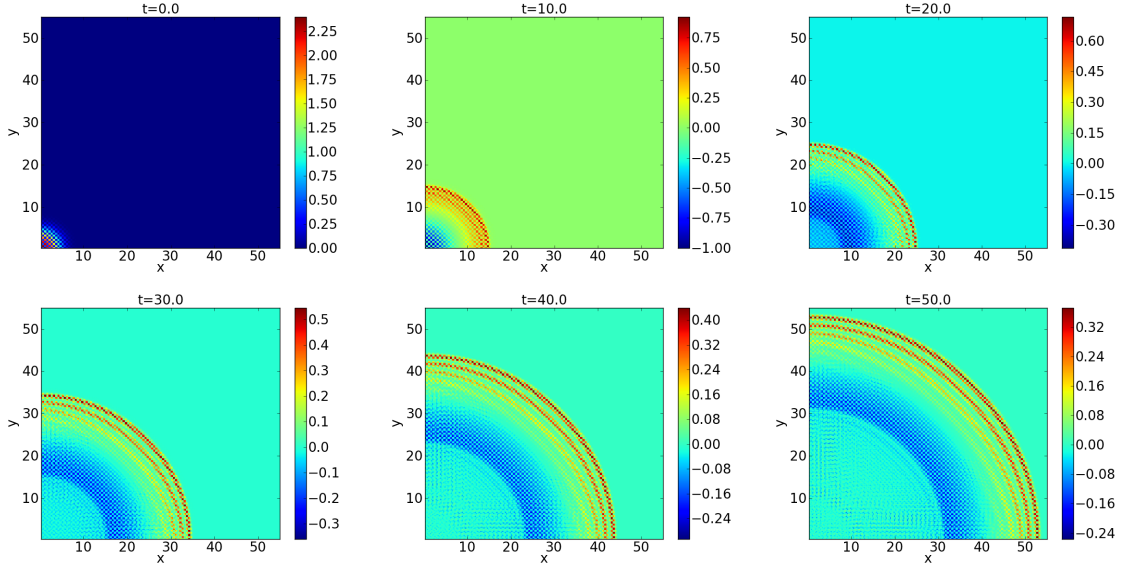


Figure IV.5.6: Evolution of strain with material parameters given by (IV.5.3). We consider $Ng=120$ grid cells per unit of the domain.

are determined by δ_y (see figure IV.1.1). The resolution is determined by considering $Ng=120$ grid cells per unit of the domain in each direction. Periodic boundary conditions are used at the top and bottom edges and absorbing walls at the left and right ones. The material parameters are:

$$E_1 = \rho_1 = 1, \quad (\text{IV.5.6a})$$

$$E_2 = \rho_2 = 10. \quad (\text{IV.5.6b})$$

When $\delta_y = 20$, the material is homogeneous in y , which corresponds to the situation in [22]. We obtain similar results. For different values of δ_y , solitary waves are also created. Nevertheless, one can easily notice having a more homogeneous medium in y enhances the stegoton formation.

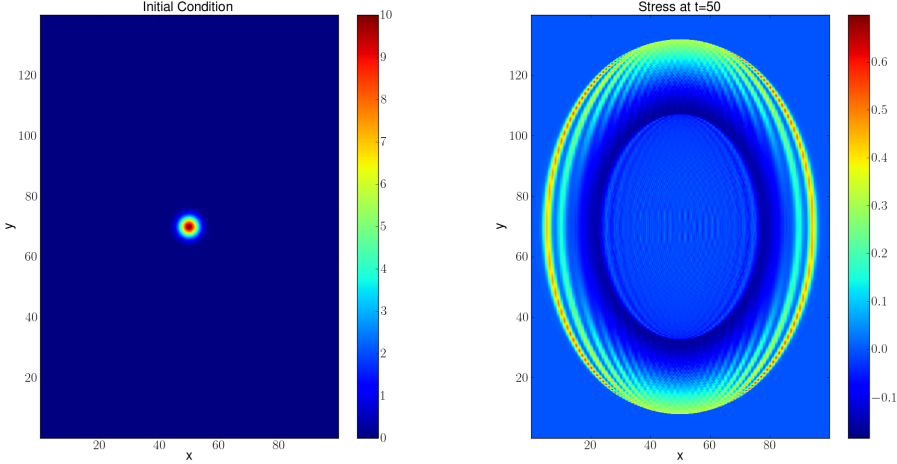


Figure IV.5.7: Initial condition (left) and stress at $t = 50$ (right) in a domain heterogeneous in x and homogeneous in y with material properties given by (IV.5.5).

IV.6 Convergence study

In the current section, we present a self-convergence study. To do so, we consider a square domain with the following properties:

$$\alpha_x = \alpha_y = 0.5, \quad (\text{IV.6.1a})$$

$$\delta_x = \delta_y = 1, \quad (\text{IV.6.1b})$$

$$E_1 = \rho_1 = 1, \quad (\text{IV.6.1c})$$

$$E_2 = \rho_2 = 5. \quad (\text{IV.6.1d})$$

and a constitutive relation given by:

$$\sigma = \exp(E\epsilon) - 1.$$

Figure IV.6.1 shows the stress at time $t = 13$ for different values of Ng ; i.e., different resolutions. The initial condition, which is a Gaussian pulse with amplitude

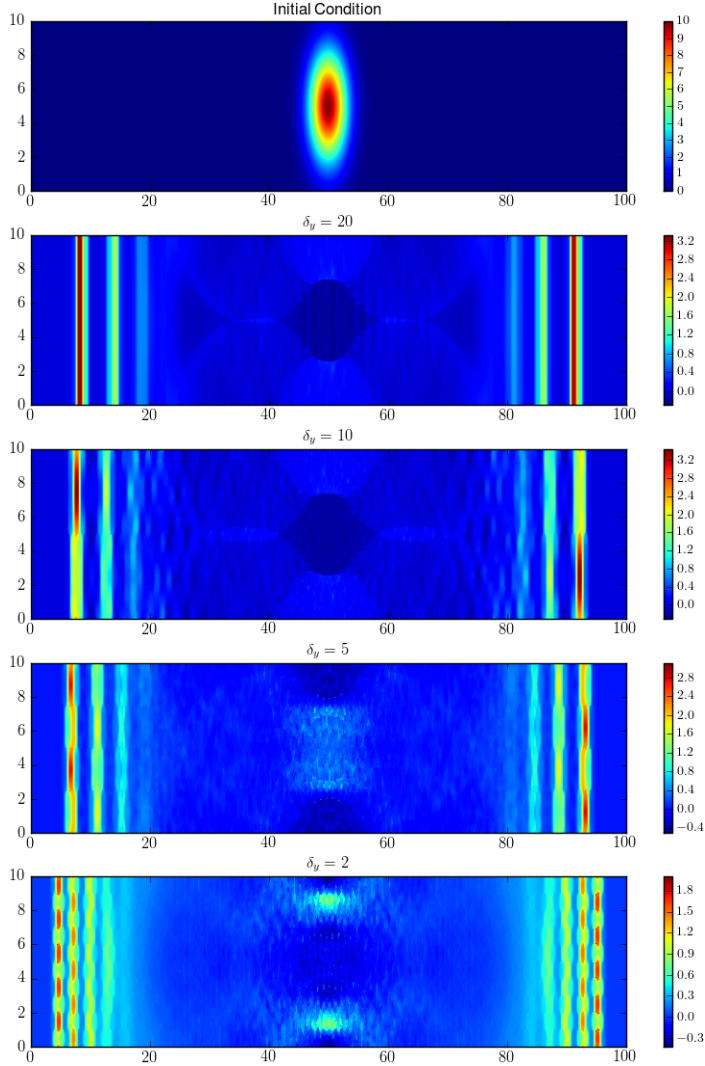


Figure IV.5.8: Initial condition (top) and stress at $t = 50$ for long thin domains with different heterogeneities in y and material properties given by (IV.5.6).

of 10 and variance in x and y of 5, is centered at the origin of the domain. Reflecting boundary conditions are implemented in all edges.

We first notice that even at this short time the solitary wave formation is starting to happen. In addition, we can see again the importance of having small numerical dissipation for the stegoton formation. Since we don't have the exact solution, we perform a self-convergence study using the solution with $\text{Ng}=960$ as “exact” solution. Figure IV.6.2 shows the corresponding convergence plot, where the relative error is used. In table IV.6.1, we present the actual computed order for each pair of resolutions

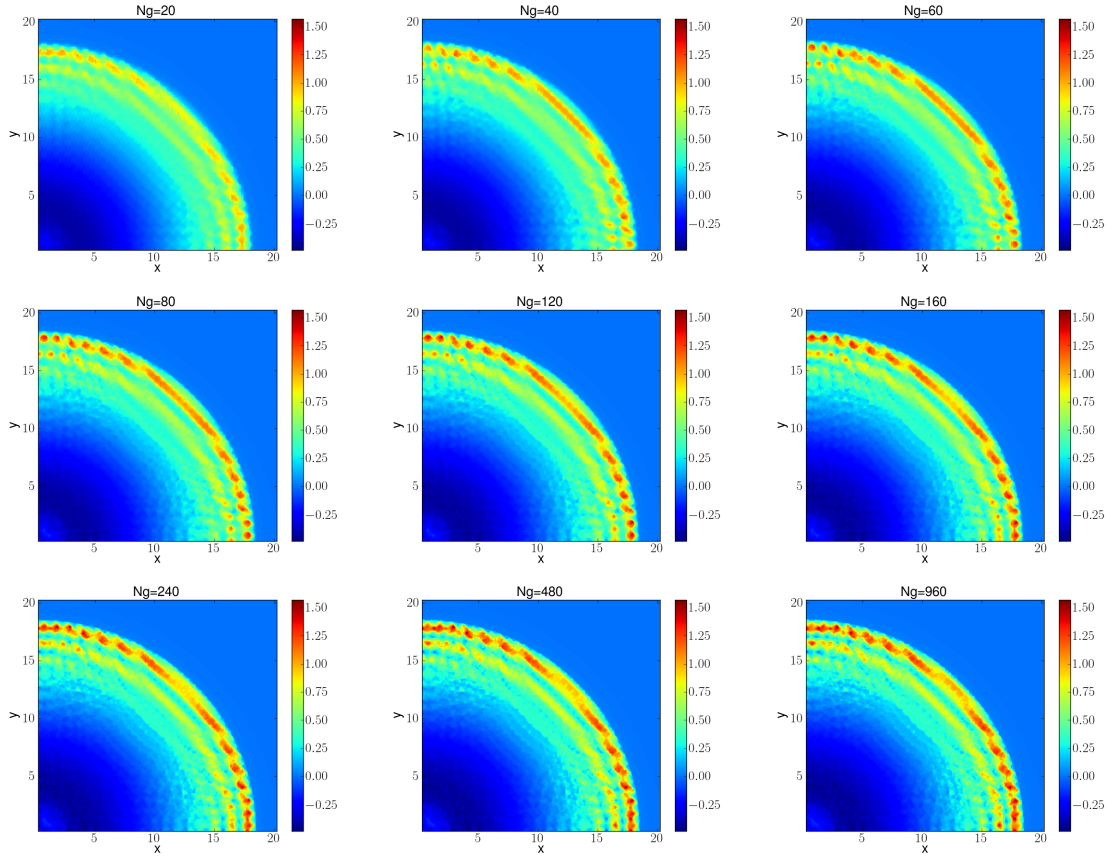


Figure IV.6.1: Stress at $t = 13$ with material parameters given by (IV.6.1) for different number of grid points.

following [23]:

$$p = \frac{\ln\left(\frac{E_f}{E_c}\right)}{\ln\left(\frac{h_f}{h_c}\right)},$$

where p is the order of accuracy, E_f and E_c are errors considering a finer and a coarser grid while h_f and h_c are the corresponding grid sizes, which are the same in x and y . We can see from figure IV.6.2 and table IV.6.1 that the achieved order of convergence tends to be slightly greater than 1.

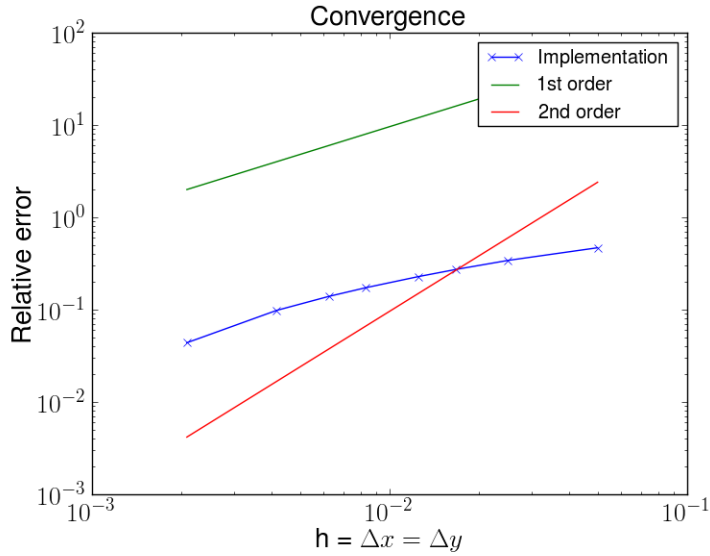


Figure IV.6.2: Self-convergence test using relative error in the grid 2-norm. All solutions used are shown in figure IV.6.1. The solution with $Ng=960$ is used as “exact” solution. The corresponding results are shown in table IV.6.1.

$Ng=\frac{1}{h}$	E	p
20	0.4683	-
40	0.3416	0.4551
60	0.2723	0.5590
80	0.2281	0.6147
120	0.1731	0.6802
160	0.1392	0.7580
240	0.0980	0.8652
480	0.0438	1.1620

Table IV.6.1: Self-convergence test using relative error in the grid 2-norm. All solutions used are shown in figure IV.6.1. The solution with $Ng=960$ is used as “exact” solution. The corresponding plot is shown in figure IV.6.2.

Part III

Homogenization

Ideally, we want to get homogenized equations for the p-system considered in Chapter IV. However, through the approach followed some difficulties arise. As a consequence, we consider a slight different system suitable for the homogenization. The system to be considered comes from the model to propagate elastic waves in 2D thin plates (see for instance [9]) where we neglect the shear stress. Doing so we get:

$$\epsilon_t^x - u_x = 0, \quad (\text{IV.6.2a})$$

$$\epsilon_t^y - v_y = 0, \quad (\text{IV.6.2b})$$

$$\rho^x u_t - \sigma_x^x = 0, \quad (\text{IV.6.2c})$$

$$\rho^y v_t - \sigma_y^y = 0, \quad (\text{IV.6.2d})$$

where ϵ^x and ϵ^y are the x - and y -component of the strain, u and v are the velocity in x and y , σ^x and σ^y are the x - and y -component of the stress and $\rho^x(x)$ and $\rho^y(y)$ are two independent components of the density, each controlling the inertial properties of the medium in one of the coordinate directions. The main difference between this model and the p-system considered in other sections is that here we consider independent x - and y -components of stress and strain; as a consequence, we now have two constitutive relations. The system is closed by introducing those constitutive relations:

$$\sigma^x = \sigma^x(\epsilon^x, \epsilon^y),$$

$$\sigma^y = \sigma^y(\epsilon^x, \epsilon^y).$$

The Young modulus of the material is considered within the constitutive relations. As the density, the Young modulus is determined by two independent components

$E^x(x)$ and $E^y(y)$, each for one direction. Figure IV.6.3 shows the characterization of the material parameters.

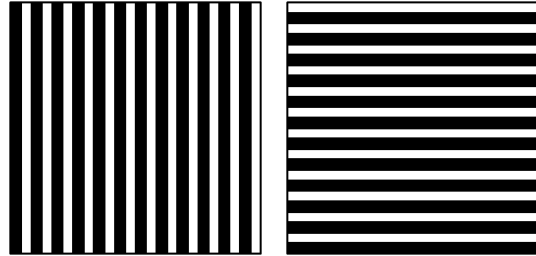


Figure IV.6.3: Representation of material parameters by the layered heterogeneity for either ρ^x or E^x (left) and for either ρ^y or E^y (right).

This part of the work is organized as follows. First, in Chapter V homogenized equations for the system (IV.6.2) are found. Afterwards, in Chapter VI the homogenized system is solved numerically and the solution is compared with the solution of (IV.6.2) obtained by finite volumes. Finally, in Chapter VII some comments regarding the stability properties of the homogenized system are discussed.

Chapter V

Derivation of homogenized equations

In this chapter, homogenized equations for the system (IV.6.2) are found following [3]. To do this, the system is inverted to find equations for the fluxes, fast spatial variables are introduced and the solutions are expanded asymptotically. Afterwards, terms of each order from $O(\delta^{-1})$ to $O(\delta^2)$, where δ is the heterogeneity period, are considered. Finally, the leading order homogenized system and the effective non-zero corrections are incorporated into a single and final system for specific constitutive relations.

V.1 Inverted system for the fluxes

First we will consider the main system (IV.6.2) and invert it to get equations for the fluxes. This is convenient since the fluxes are continuous, see [5] for a 1D version. Recall the system (IV.6.2):

$$\epsilon_t^x - u_x = 0, \quad (\text{V.1.1a})$$

$$\epsilon_t^y - v_y = 0, \quad (\text{V.1.1b})$$

$$\rho^x u_t - \sigma_x^x = 0, \quad (\text{V.1.1c})$$

$$\rho^y v_t - \sigma_y^y = 0. \quad (\text{V.1.1d})$$

The system is closed by introducing the constitutive relations:

$$\sigma^x = \sigma^x(\epsilon^x, \epsilon^y), \quad (\text{V.1.2a})$$

$$\sigma^y = \sigma^y(\epsilon^x, \epsilon^y). \quad (\text{V.1.2b})$$

Using the chain rule in (V.1.2), we obtain:

$$\sigma_t^x = \sigma_{\epsilon^x}^x \epsilon_t^x + \sigma_{\epsilon^y}^x \epsilon_t^y, \quad (\text{V.1.3a})$$

$$\sigma_t^y = \sigma_{\epsilon^x}^y \epsilon_t^x + \sigma_{\epsilon^y}^y \epsilon_t^y. \quad (\text{V.1.3b})$$

Multiplying (V.1.1a) by $\sigma_{\epsilon^x}^x$ and (V.1.1b) by $\sigma_{\epsilon^y}^y$ and using (V.1.1a), (V.1.1b) and (V.1.3), we get:

$$\sigma_t^x - \sigma_{\epsilon^x}^x u_x - \sigma_{\epsilon^y}^x v_y = 0, \quad (\text{V.1.4a})$$

$$\sigma_t^y - \sigma_{\epsilon^y}^y v_y - \sigma_{\epsilon^x}^y u_x = 0. \quad (\text{V.1.4b})$$

Based on [5], we assume:

$$\sigma_{\epsilon^x}^x = E^x(x) P(\sigma^x), \quad (\text{V.1.5a})$$

$$\sigma_{\epsilon^y}^x = E^y(y) Q(\sigma^x), \quad (\text{V.1.5b})$$

$$\sigma_{\epsilon^y}^y = E^y(y) R(\sigma^y), \quad (\text{V.1.5c})$$

$$\sigma_{\epsilon^x}^y = E^x(x) S(\sigma^y), \quad (\text{V.1.5d})$$

where E^x and E^y are periodic functions in x and y that characterize the variable Young modulus of the material. Plugging (V.1.5) into (V.1.4), results in:

$$(E^x E^y)^{-1} \sigma_t^x - (E^y)^{-1} P(\sigma^x) u_x - (E^x)^{-1} Q(\sigma^x) v_y = 0, \quad (\text{V.1.6a})$$

$$(E^x E^y)^{-1} \sigma_t^y - (E^x)^{-1} R(\sigma^y) v_y - (E^y)^{-1} S(\sigma^y) u_x = 0, \quad (\text{V.1.6b})$$

which along with:

$$\rho^x u_t - \sigma_x^x = 0, \quad (\text{V.1.6c})$$

$$\rho^y v_t - \sigma_y^y = 0, \quad (\text{V.1.6d})$$

represent the inverted system.

V.2 Asymptotic expansion

To take into account the fast change in material properties, we introduce the fast spatial variables:

$$\begin{aligned}\hat{x} &= \frac{x}{\delta}, \\ \hat{y} &= \frac{y}{\gamma\delta},\end{aligned}$$

where $\delta \ll 1$ is the length of the unit cell in \hat{x} or \hat{y} and $\gamma = O(1)$ allows the heterogeneity in each direction to be different but of the same order. We assume that since the material properties are changing fast, they are function of the fast variables; i.e., $E^x = E^x(\hat{x})$, $E^y = E^y(\hat{y})$, $\rho^x = \rho(\hat{x})$ and $\rho^y = \rho(\hat{y})$. In addition, we introduce these fast spatial variables to the system to get $u = u(x, \hat{x}, y, \hat{y}, t)$, $v = v(x, \hat{x}, y, \hat{y}, t)$, $\sigma^x = \sigma^x(x, \hat{x}, y, \hat{y}, t)$ and $\sigma^y = \sigma^y(x, \hat{x}, y, \hat{y}, t)$. The operators are changed accordingly using the chain rule so that $(\cdot)_x \rightarrow (\cdot)_x + \delta^{-1}(\cdot)_{\hat{x}}$ and $(\cdot)_y \rightarrow (\cdot)_y + \gamma^{-1}\delta^{-1}(\cdot)_{\hat{y}}$. Finally, the inverted system becomes:

$$(E^x E^y)^{-1} \sigma_t^x - (E^y)^{-1} P(\sigma^x)(u_x + \delta^{-1}u_{\hat{x}}) \quad (V.2.1a)$$

$$- (E^x)^{-1} Q(\sigma^x)(v_y + \gamma^{-1}\delta^{-1}v_{\hat{y}}) = 0,$$

$$(E^x E^y)^{-1} \sigma_t^y - (E^x)^{-1} R(\sigma^y)(v_y + \gamma^{-1}\delta^{-1}v_{\hat{y}}) \quad (V.2.1b)$$

$$- (E^y)^{-1} S(\sigma^y)(u_x + \delta^{-1}u_{\hat{x}}) = 0,$$

$$\rho^x u_t - \sigma_x^x - \delta^{-1} \sigma_{\hat{x}}^x = 0, \quad (V.2.1c)$$

$$\rho^y v_t - \sigma_y^y - \gamma^{-1}\delta^{-1} \sigma_{\hat{y}}^y = 0, \quad (V.2.1d)$$

which represents the inverted system with fast spatial variables due to fast change of the coefficients.

We expand the variables in δ :

$$u = \sum_{i=0}^{\infty} \delta^i u_i(x, \hat{x}, y, \hat{y}, t), \quad v = \sum_{i=0}^{\infty} \delta^i v_i(x, \hat{x}, y, \hat{y}, t), \quad (\text{V.2.2a})$$

$$\sigma^x = \sum_{i=0}^{\infty} \delta^i \sigma_i^x(x, \hat{x}, y, \hat{y}, t), \quad \sigma^y = \sum_{i=0}^{\infty} \delta^i \sigma_i^y(x, \hat{x}, y, \hat{y}, t), \quad (\text{V.2.2b})$$

and use Taylor series to expand the functions of σ^x and σ^y around σ_0^x and σ_0^y respectively; e.g.:

$$P(\sigma^x) = \sum_{i=0}^{\infty} \frac{P^{(i)}(\sigma_0^x)}{i!} \left(\sum_{j=1}^{\infty} \delta^j \sigma_j^x \right)^i.$$

V.3 Terms of $O(\delta^{-1})$

Collecting terms of $O(\delta^{-1})$ in equations (V.2.1a) and (V.2.1b) expanded via (V.2.2) and the expansions of $P(\sigma^x)$, $Q(\sigma^x)$, $R(\sigma^y)$ and $S(\sigma^y)$ yields:

$$\begin{bmatrix} (E^y)^{-1} P(\sigma_0^x) & \gamma^{-1} (E^x)^{-1} Q(\sigma_0^x) \\ (E^y)^{-1} S(\sigma_0^y) & \gamma^{-1} (E^x)^{-1} R(\sigma_0^y) \end{bmatrix} \begin{bmatrix} u_{0,\hat{x}} \\ v_{0,\hat{y}} \end{bmatrix} = \begin{bmatrix} 0 \\ 0 \end{bmatrix}.$$

If we assume the matrix is non-singular; i.e., $P(\sigma_0^x)R(\sigma_0^y) \neq Q(\sigma_0^x)S(\sigma_0^y)$, then $u_{0,\hat{x}} = v_{0,\hat{y}} = 0$ yields:

$$u_0 = u_0(x, y, \hat{y}, t), \quad v_0 = v_0(x, \hat{x}, y, t).$$

Similarly, from the $O(\delta^{-1})$ equations in (V.2.1c) and (V.2.1d) one can conclude:

$$\sigma_0^x = \sigma_0^x(x, y, \hat{y}, t), \quad \sigma_0^y = \sigma_0^y(x, \hat{x}, y, t).$$

At this point, we must extend this conclusion and assume any leading order solution is not a function of the fast variables, which is a fair assumption following

homogenization ideas. By doing this, we get:

$$u_0 \equiv U_0(x, y, t), \quad v_0 \equiv V_0(x, y, t),$$

$$\sigma_0^x \equiv \Sigma_0^x(x, y, t), \quad \sigma_0^y \equiv \Sigma_0^y(x, y, t),$$

where we use upper case letters for the solution variables that are not function of \hat{x} or \hat{y} . Thus, from the $O(\delta^{-1})$ section we just conclude that the leading order solution doesn't depend on the fast variables, under the assumption taken.

V.4 Terms of $O(1)$

In this section, we first gather terms of $O(1)$ and find a homogenized leading order system. Afterwards, we decompose u_1 , v_1 , σ_1^x and σ_1^y so that after plugging them into the $O(1)$ system we obtain ODEs that define them.

The system of $O(1)$ is:

$$(E^x E^y)^{-1} \Sigma_{0,t}^x - (E^y)^{-1} P(\Sigma_0^x) (U_{0,x} + u_{1,\hat{x}}) - (E^x)^{-1} Q(\Sigma_0^x) (V_{0,y} + \gamma^{-1} v_{1,\hat{y}}) = 0, \quad (\text{V.4.1a})$$

$$(E^x E^y)^{-1} \Sigma_{0,t}^y - (E^x)^{-1} R(\Sigma_0^y) (V_{0,y} + \gamma^{-1} v_{1,\hat{y}}) - (E^y)^{-1} S(\Sigma_0^y) (U_{0,x} + u_{1,\hat{x}}) = 0, \quad (\text{V.4.1b})$$

$$\rho U_{0,t} - \Sigma_{0,x}^x - \sigma_{1,\hat{x}}^x = 0, \quad (\text{V.4.1c})$$

$$\rho V_{0,t} - \Sigma_{0,y}^y - \gamma^{-1} \sigma_{1,\hat{y}}^y = 0. \quad (\text{V.4.1d})$$

V.4.1 Averaged $O(1)$ system

We apply the averaging operator $\langle \cdot \rangle$ from (II.0.1) to (V.4.1) assuming that $\langle \phi_{\hat{x}} \rangle = \langle \phi_{\hat{y}} \rangle \equiv 0$ for any function ϕ periodic on a unit cell (see Chapter II for details on these and other homogenization concepts). Doing so we obtain:

$$E_h^x E_h^y \Sigma_{0,t}^x = E_h^y P(\Sigma_0^x) U_{0,x} + E_h^x Q(\Sigma_0^x) V_{0,y}, \quad (\text{V.4.2a})$$

$$E_h^x E_h^y \Sigma_{0,t}^y = E_h^x R(\Sigma_0^y) V_{0,y} + E_h^y S(\Sigma_0^y) U_{0,x}, \quad (\text{V.4.2b})$$

$$\rho_h^x U_{0,t} = \Sigma_{0,x}^x, \quad (\text{V.4.2c})$$

$$\rho_h^y V_{0,t} = \Sigma_{0,y}^y. \quad (\text{V.4.2d})$$

where we use the notation $E_h^x = \langle E^x \rangle$ and similarly for E_h^y , ρ_h^x and ρ_h^y . This system represents the homogenized leading order system. It has the form of the inverted system with constant material properties defined by average quantities.

V.4.2 Ansatz for $O(1)$ system

Based on [3], we propose the following ansatz for the $O(1)$ system (V.4.1):

$$u_1 = U_1(x, y, t) + A(\hat{x}) U_{0,x}(x, y, t), \quad (\text{V.4.3a})$$

$$v_1 = V_1(x, y, t) + B(\hat{y}) V_{0,y}(x, y, t), \quad (\text{V.4.3b})$$

$$\sigma_1^x = \Sigma_1^x(x, y, t) + C(\hat{x}) \Sigma_{0,x}^x(x, y, t), \quad (\text{V.4.3c})$$

$$\sigma_1^y = \Sigma_1^y(x, y, t) + D(\hat{y}) \Sigma_{0,y}^y(x, y, t). \quad (\text{V.4.3d})$$

Plug this ansatz into (V.4.1a) and use the homogenized leading order equation (V.4.2a) to get:

$$\begin{aligned} & P(\Sigma_0^x) U_{0,x} (E^y)^{-1} \left[(E^x)^{-1} (E_h^x)^{-1} - 1 - A_{\hat{x}} \right] \\ & + Q(\Sigma_0^x) V_{0,y} (E^x)^{-1} \left[(E^y)^{-1} (E_h^y)^{-1} - 1 - \gamma^{-1} B_{\hat{y}} \right] = 0, \end{aligned}$$

from where we let:

$$A_{\hat{x}} = (E^x)^{-1} (E_h^x)^{-1} - 1, \quad (\text{V.4.4a})$$

$$B_{\hat{y}} = \gamma \left[(E^y)^{-1} (E_h^y)^{-1} - 1 \right]. \quad (\text{V.4.4b})$$

The same can be obtained if we consider (V.4.1b) instead of (V.4.1a). Similarly, considering the $O(1)$ equations (V.4.1c) and (V.4.1d), the ansatz (V.4.3) and the homogenized leading order equations (V.4.2), we obtain:

$$C_{\hat{x}} = \rho^x (\rho_h^x)^{-1} - 1, \quad (\text{V.4.5a})$$

$$D_{\hat{y}} = \gamma \left[\rho^y (\rho_h^y)^{-1} - 1 \right]. \quad (\text{V.4.5b})$$

If we consider piecewise constant material properties, we can split $A(\hat{x})$ in two parts, which yields:

$$\begin{aligned} A_{1,\hat{x}} &= (E_1^x)^{-1} (E_h^x)^{-1} - 1, \quad \hat{x} \in [0, \alpha_x], \\ A_{2,\hat{x}} &= (E_2^x)^{-1} (E_h^x)^{-1} - 1, \quad \hat{x} \in [\alpha_x, 1]. \end{aligned}$$

From homogenization ideas (see Chapter II), we impose continuity and normalization on A ; i.e., $A_1(\alpha_x) = A_2(\alpha_x)$ and $\langle A(\hat{x}) \rangle = 0$ respectively. Doing so, we

get:

$$A(\hat{x}) = \begin{cases} A_1(\hat{x}) = \frac{(1-\alpha_x)(E_2^x - E_1^x)}{(1-\alpha_x)E_1^x + \alpha_x E_2^x} \left(\hat{x} - \frac{\alpha_x}{2} \right), & \hat{x} \in [0, \alpha_x] \\ A_2(\hat{x}) = \frac{\alpha_x(E_2^x - E_1^x)}{(1-\alpha_x)E_1^x + \alpha_x E_2^x} \left(\frac{1+\alpha_x}{2} - \hat{x} \right), & \hat{x} \in [\alpha_x, 1] \end{cases}.$$

In a similar way, $B(\hat{y})$ is split as:

$$\begin{aligned} B_{1,\hat{y}} &= \gamma \left[(E_1^y)^{-1} (E_h^y)^{-1} - 1 \right], \quad \hat{y} \in [0, \alpha_y], \\ B_{2,\hat{y}} &= \gamma \left[(E_2^y)^{-1} (E_h^y)^{-1} - 1 \right], \quad \hat{y} \in [\alpha_y, 1], \end{aligned}$$

and imposing continuity and normalization we find:

$$B(\hat{y}) = \begin{cases} B_1(\hat{y}) = \gamma \frac{(1-\alpha_y)(E_2^y - E_1^y)}{(1-\alpha_y)E_1^y + \alpha_y E_2^y} \left(\hat{y} - \frac{\alpha_y}{2} \right), & \hat{y} \in [0, \alpha_y] \\ B_2(\hat{y}) = \gamma \frac{\alpha_y(E_2^y - E_1^y)}{(1-\alpha_y)E_1^y + \alpha_y E_2^y} \left(\frac{1+\alpha_y}{2} - \hat{y} \right), & \hat{y} \in [\alpha_y, 1] \end{cases}.$$

Splitting the function $C(\hat{x})$ yields:

$$\begin{aligned} C_{1,\hat{x}}(\hat{x}) &= \rho_1^x (\rho_h^x)^{-1} - 1, \quad \hat{x} \in [0, \alpha_x], \\ C_{2,\hat{x}}(\hat{x}) &= \rho_2^x (\rho_h^x)^{-1} - 1, \quad \hat{x} \in [\alpha_x, 1], \end{aligned}$$

whose respective solution, after imposing continuity and normalization, is:

$$C(\hat{x}) = \begin{cases} C_1(\hat{x}) = \frac{(1-\alpha_x)(\rho_1^x - \rho_2^x)}{\alpha_x \rho_1^x + (1-\alpha_x) \rho_2^x} \left(\hat{x} - \frac{\alpha_x}{2} \right), & \hat{x} \in [0, \alpha_x] \\ C_2(\hat{x}) = \frac{\alpha_x(\rho_1^x - \rho_2^x)}{\alpha_x \rho_1^x + (1-\alpha_x) \rho_2^x} \left(\frac{1+\alpha_x}{2} - \hat{x} \right), & \hat{x} \in [\alpha_x, 1] \end{cases}.$$

Finally, $D(\hat{y})$ is split as:

$$\begin{aligned} D_{1,\hat{y}}(\hat{y}) &= \gamma \left[\rho^y (\rho_h^y)^{-1} - 1 \right], \quad \hat{y} \in [0, \alpha_y], \\ D_{2,\hat{y}}(\hat{y}) &= \gamma \left[\rho^y (\rho_h^y)^{-1} - 1 \right], \quad \hat{y} \in [\alpha_y, 1], \end{aligned}$$

where we impose continuity and normalization and find:

$$D(\hat{y}) = \begin{cases} D_1(\hat{y}) = \gamma \frac{(1-\alpha_y)(\rho_1^y - \rho_2^y)}{\alpha_y \rho_1^y + (1-\alpha_y) \rho_2^y} \left(\hat{y} - \frac{\alpha_y}{2} \right), & \hat{y} \in [0, \alpha_y] \\ D_2(\hat{y}) = \gamma \frac{\alpha_y(\rho_1^y - \rho_2^y)}{\alpha_y \rho_1^y + (1-\alpha_y) \rho_2^y} \left(\frac{1+\alpha_y}{2} - \hat{y} \right), & \hat{y} \in [\alpha_y, 1] \end{cases}.$$

It is important to remember that these functions are continuous and normalized so that:

$$\langle A(\hat{x}) \rangle = \langle B(\hat{y}) \rangle = \langle C(\hat{x}) \rangle = \langle D(\hat{y}) \rangle = 0, \quad (\text{V.4.6})$$

along with the fact that:

$$\langle A_{\hat{x}}(\hat{x}) \rangle = \langle B_{\hat{y}}(\hat{y}) \rangle = \langle C_{\hat{x}}(\hat{x}) \rangle = \langle D_{\hat{y}}(\hat{y}) \rangle = 0, \quad (\text{V.4.7})$$

which implies periodicity on them and, hence, on u_1 , v_1 , σ_1^x and σ_2^y with respect to the respective fast variables as assumed before. These expressions will be required in future corrections.

V.5 Terms of $O(\delta)$

This section goes as the previous one. We first gather terms of $O(\delta)$ and apply the double average operator $\langle \cdot \rangle$ to find effective equations; namely, the first homogenized correction. Afterwards, we decompose u_2 , v_2 , σ_2^x and σ_2^y to get ODEs that define them.

The system of order $O(\delta)$ is:

$$(E^x E^y)^{-1} \sigma_{1,t}^x - (E^y)^{-1} P(\Sigma_0^x) (u_{1,x} + u_{2,\hat{x}}) \quad (\text{V.5.1a})$$

$$- (E^y)^{-1} P'(\Sigma_0^x) \sigma_1^x (U_{0,x} + u_{1,\hat{x}})$$

$$- (E^x)^{-1} Q(\Sigma_0^x) (v_{1,y} + \gamma^{-1} v_{2,\hat{y}})$$

$$- (E^x)^{-1} Q'(\Sigma_0^x) \sigma_1^x (V_{0,y} + \gamma^{-1} v_{1,\hat{y}}) = 0,$$

$$(E^x E^y)^{-1} \sigma_{1,t}^y - (E^x)^{-1} R(\Sigma_0^y) (v_{1,y} + \gamma^{-1} v_{2,\hat{y}}) \quad (\text{V.5.1b})$$

$$- (E^x)^{-1} R'(\Sigma_0^y) \sigma_1^y (V_{0,y} + \gamma^{-1} v_{1,\hat{y}})$$

$$- (E^y)^{-1} S(\Sigma_0^y) (u_{1,x} + u_{2,\hat{x}})$$

$$- (E^y)^{-1} S'(\Sigma_0^y) \sigma_1^y (U_{0,x} + u_{1,\hat{x}}) = 0,$$

$$\rho^x u_{1,t} - \sigma_{1,x}^x - \sigma_{2,\hat{x}}^x = 0, \quad (\text{V.5.1c})$$

$$\rho^y v_{1,t} - \sigma_{1,y}^y - \gamma^{-1} \sigma_{2,\hat{y}}^y = 0. \quad (\text{V.5.1d})$$

V.5.1 Averaged $O(\delta)$ system

We apply the average operator $\langle \cdot \rangle$ to the $O(\delta)$ system to get:

$$E_h^x E_h^y \Sigma_{1,t}^x = E_h^y P(\Sigma_0^x) U_{1,x} + E_h^x Q(\Sigma_0^x) V_{1,y} \quad (\text{V.5.2a})$$

$$= +\Sigma_1^x [E_h^y P'(\Sigma_0^x) U_{0,x} + E_h^x Q'(\Sigma_0^x) V_{0,y}],$$

$$E_h^x E_h^y \Sigma_{1,t}^y = E_h^x R(\Sigma_0^y) V_{1,y} + E_h^y S(\Sigma_0^y) U_{1,x} \quad (\text{V.5.2b})$$

$$+ \Sigma_1^y [E_h^x R'(\Sigma_0^y) V_{0,y} + E_h^y S'(\Sigma_0^y) U_{0,x}],$$

$$\rho_h^x U_{1,t} = \Sigma_{1,x}^x, \quad (\text{V.5.2c})$$

$$\rho_h^y V_{1,t} = \Sigma_{1,y}^y, \quad (\text{V.5.2d})$$

where the following computations were required:

$$\begin{aligned}\langle (E^x E^y)^{-1} C(\hat{x}) \rangle &= \langle C(\hat{x}) A_{\hat{x}}(\hat{x}) \rangle = \langle C(\hat{x}) B_{\hat{y}}(\hat{y}) \rangle = 0, \\ \langle (E^x E^y)^{-1} D(\hat{y}) \rangle &= \langle D(\hat{y}) B_{\hat{y}}(\hat{y}) \rangle = \langle D(\hat{y}) A_{\hat{x}}(\hat{x}) \rangle = 0, \\ \langle \rho^x A(\hat{x}) \rangle &= \langle \rho^y B(\hat{y}) \rangle = 0,\end{aligned}$$

among with the normalization and periodicity conditions expressed by (V.4.6) and (V.4.7) respectively.

The boundary and initial conditions are considered in the homogenized leading order. Therefore, they are zero for the homogenized corrections. Considering, in addition, that the homogenized first correction (V.5.2) is unforced, we conclude the solution vanishes; i.e.:

$$U_1 = V_1 = \Sigma_1^x = \Sigma_1^y = 0.$$

V.5.2 Ansatz for $O(\delta)$ system

Now, we propose an ansatz for the $O(\delta)$ system (V.5.1), plug it into the $O(\delta)$ system and use the homogenized leading order and first correction to get ODEs that define the proposed ansatz. We let:

$$u_2 = U_2(x, y, t) + A(\hat{x}) U_{1,x}(x, y, t) + F(\hat{x}) U_{0,xx}(x, y, t), \quad (\text{V.5.3a})$$

$$v_2 = V_2(x, y, t) + B(\hat{y}) V_{1,y}(x, y, t) + G(\hat{y}) V_{0,yy}(x, y, t), \quad (\text{V.5.3b})$$

$$\sigma_2^x = \Sigma_2^x(x, y, t) + C(\hat{x}) \Sigma_{1,x}^x(x, y, t) + H(\hat{x}) \Sigma_{0,xx}^x(x, y, t), \quad (\text{V.5.3c})$$

$$\sigma_2^y = \Sigma_2^y(x, y, t) + D(\hat{y}) \Sigma_{1,y}^y(x, y, t) + I(\hat{y}) \Sigma_{0,yy}^y(x, y, t). \quad (\text{V.5.3d})$$

Plug the ansatz for u_2 , v_2 and σ_2^x from (V.5.3a)-(V.5.3c), the ansatz for u_1 , v_1 and σ_1^x from (V.4.3a)-(V.4.3c), the homogenized first correction and the expressions for $A_{\hat{x}}$ and $B_{\hat{y}}$ from (V.4.4) into (V.5.1a) to get:

$$\begin{aligned} & - (E^y)^{-1} P(\Sigma_0^x) U_{0,xx} (A + F_{\hat{x}}) - (E^x)^{-1} Q(\Sigma_0^x) V_{0,yy} (B + \gamma^{-1} G_{\hat{y}}) \quad (\text{V.5.4}) \\ & + (E^x E^y)^{-1} C \left\{ \Sigma_{0,xt}^x - \left[(E_h^x)^{-1} P'(\Sigma_0^x) U_{0,x} + (E_h^y)^{-1} Q'(\Sigma_0^x) V_{0,y} \right] \Sigma_{0,x}^x \right\} = 0. \end{aligned}$$

We use the homogenized first correction, differentiate it with respect to x and plug it into (V.5.4) to get:

$$\begin{aligned} & (E^y)^{-1} P(\Sigma_0^x) U_{0,xx} [(E^x)^{-1} (E_h^x)^{-1} C - A - F_{\hat{x}}] \quad (\text{V.5.5}) \\ & - (E^x)^{-1} Q(\Sigma_0^x) V_{0,yy} (B + \gamma^{-1} G_{\hat{y}}) + (E^x E^y)^{-1} (E_h^y)^{-1} C Q(\Sigma_0^x) V_{0,xy} = 0. \end{aligned}$$

Considering (V.5.1b) instead and following similar steps we obtain:

$$\begin{aligned} & (E^x)^{-1} R(\Sigma_0^y) V_{0,yy} \left[(E^y)^{-1} (E_h^y)^{-1} D - B - \gamma^{-1} G_{\hat{y}} \right] \quad (\text{V.5.6}) \\ & - (E^y)^{-1} S(\Sigma_0^y) U_{0,xx} (A + F_{\hat{x}}) + (E^x E^y)^{-1} (E_h^x)^{-1} D S(\Sigma_0^y) U_{0,xy} = 0. \end{aligned}$$

At this point, we expected to get ODEs for F and G . However, the terms $(E^x E^y)^{-1} (E_h^y)^{-1} C Q(\Sigma_0^x) V_{0,xy}$ and $(E^x E^y)^{-1} (E_h^x)^{-1} D S(\Sigma_0^y) U_{0,xy}$ in (V.5.5) and (V.5.6) respectively break up the symmetry making not possible to get the desired ODEs using the current ansatz. As a consequence, we modify the ansatz for u_2 and v_2 so that we obtain the mentioned ODEs. The new ansatz is:

$$u_2 = U_2(x, y, t) + A(\hat{x}) U_{1,x}(x, y, t) \quad (\text{V.5.7a})$$

$$+ F(\hat{x}) U_{0,xx}(x, y, t) + J(x, \hat{x}, y, \hat{y}, t),$$

$$v_2 = V_2(x, y, t) + B(\hat{y}) V_{1,y}(x, y, t) \quad (\text{V.5.7b})$$

$$+ G(\hat{y}) V_{0,yy}(x, y, t) + K(x, \hat{x}, y, \hat{y}, t).$$

To find out what are the correct $J(x, \hat{x}, y, \hat{y}, t)$ and $K(x, \hat{x}, y, \hat{y}, t)$ functions we plug (V.5.7), (V.5.3c) and (V.5.3d) into the $O(\delta)$ equations (V.5.1a) and (V.5.1b) and find two algebraic linear equations for $J_{\hat{x}}$ and $K_{\hat{y}}$ that allow us to get the desired ODEs for $F(\hat{x})$ and $G(\hat{y})$. The linear system is:

$$\begin{bmatrix} E^x P(\Sigma_0^x) & \gamma^{-1} E^y Q(\Sigma_0^x) \\ E^x S(\Sigma_0^y) & \gamma^{-1} E^y R(\Sigma_0^y) \end{bmatrix} \begin{bmatrix} J_{\hat{x}} \\ K_{\hat{y}} \end{bmatrix} = \begin{bmatrix} (E_h^y)^{-1} Q(\Sigma_0^x) [CV_{0,xy} - DV_{0,yy}] \\ (E_h^x)^{-1} S(\Sigma_0^y) [DU_{0,xy} - CU_{0,xx}] \end{bmatrix},$$

which has a unique solution if $P(\Sigma_0^x) R(\Sigma_0^y) \neq Q(\Sigma_0^x) S(\Sigma_0^y)$. Assuming this is the case, we get:

$$J_{\hat{x}} = (E^x)^{-1} D(\hat{y}) \chi_1(x, y, t) + (E^x)^{-1} C(\hat{x}) \chi_2(x, y, t),$$

$$K_{\hat{y}} = \gamma [(E^y)^{-1} C(\hat{x}) \chi_3(x, y, t) + (E^y)^{-1} D(\hat{y}) \chi_4(x, y, t)],$$

where:

$$\begin{aligned}
\chi_1 &= \frac{-Q(\Sigma_0^x)}{\Delta} \left[(E_h^y)^{-1} R(\Sigma_0^y) V_{o,yy} + (E_h^x)^{-1} S(\Sigma_0^y) U_{0,xy} \right], \\
\chi_2 &= \frac{Q(\Sigma_0^x)}{\Delta} \left[(E_h^y)^{-1} R(\Sigma_0^y) V_{o,xy} + (E_h^x)^{-1} S(\Sigma_0^y) U_{0,xx} \right], \\
\chi_3 &= \frac{-S(\Sigma_0^y)}{\Delta} \left[(E_h^y)^{-1} Q(\Sigma_0^x) V_{o,xy} + (E_h^x)^{-1} P(\Sigma_0^x) U_{0,xx} \right], \\
\chi_4 &= \frac{S(\Sigma_0^y)}{\Delta} \left[(E_h^y)^{-1} Q(\Sigma_0^x) V_{o,yy} + (E_h^x)^{-1} P(\Sigma_0^x) U_{0,xy} \right],
\end{aligned}$$

where $\Delta = P(\Sigma_0^x) R(\Sigma_0^y) - Q(\Sigma_0^x) S(\Sigma_0^y)$.

We impose continuity and normalization conditions on J and K . More important than the actual expressions is to remember they are continuous, their normalization condition is:

$$\langle J \rangle = \langle K \rangle = 0,$$

and are periodic, which can be shown by:

$$\langle J_{\hat{x}} \rangle = \langle K_{\hat{y}} \rangle = 0. \quad (\text{V.5.8})$$

Finally, out of this process we are able to get the desired ODEs for $F(\hat{x})$ and $G(\hat{y})$:

$$\begin{aligned}
F_{\hat{x}} &= (E^x)^{-1} (E_h^x)^{-1} C(\hat{x}) - A(\hat{x}), \\
G_{\hat{y}} &= \gamma \left[(E^y)^{-1} (E_h^y)^{-1} D(\hat{y}) - B(\hat{y}) \right].
\end{aligned}$$

Assuming piecewise constant materials, we split $F(\hat{x})$ and get ODEs for $F_1(\hat{x})$ and $F_2(\hat{x})$. As usual, continuity and normalization conditions are imposed. Doing this we find:

$$F(\hat{x}) = \begin{cases} F_1(\hat{x}) = f_{12}\hat{x}^2 + f_{11}\hat{x} + f_{10}, & \hat{x} \in [0, \alpha_x] \\ F_2(\hat{x}) = f_{22}\hat{x}^2 + f_{21}\hat{x} + f_{20}, & \hat{x} \in [\alpha_x, 1] \end{cases}, \quad (\text{V.5.9})$$

where the f' s are known constants omitted here since they become cumbersome. In a similar way, the function $G(\hat{y})$ is split and solved imposing continuity and normalization.

Plug the ansatz for σ_2^x from (V.5.3c), the ansatz for u_1 and σ_1^x from (V.4.3a) and (V.4.3c) respectively, the homogenized first correction and the expression for $C_{\hat{x}}$ from (V.4.5a) into (V.5.1c) to get:

$$\rho^x A U_{0,xt} - \Sigma_{0,xx}^x (C + H_{\hat{x}}) = 0. \quad (\text{V.5.10})$$

Use the homogenized leading order equation (V.4.2c), differentiate it with respect to x and plug it into (V.5.10) to get:

$$H_{\hat{x}} = \rho^x (\rho_n^x)^{-1} A(\hat{x}) - C(\hat{x}),$$

which is solved after splitting it into two subdomains and impose the usual continuity and normalization conditions.

Similarly, considering (V.5.1d) instead of (V.5.1c), we obtain:

$$I_{\hat{y}} = \gamma \left[\rho^y (\rho_h^y)^{-1} B(\hat{y}) - D(\hat{y}) \right],$$

whose solution is found in a similar way imposing its respective conditions.

The expressions for $G(\hat{y})$, $H(\hat{x})$ and $I(\hat{y})$ are not shown here since they have the same form as (V.5.9). As usual, it is important to remember they are continuous, their normalization condition is:

$$\langle F(\hat{x}) \rangle = \langle G(\hat{y}) \rangle = \langle H(\hat{x}) \rangle = \langle I(\hat{y}) \rangle = 0,$$

and that they are periodic, which can be shown by computing:

$$\langle F_{\hat{x}}(\hat{x}) \rangle = \langle G_{\hat{y}}(\hat{y}) \rangle = \langle H_{\hat{x}}(\hat{x}) \rangle = \langle I_{\hat{y}}(\hat{y}) \rangle = 0,$$

which along with (V.5.8) implies periodicity of u_2 , v_2 , σ^x and σ^y with respect to the fast variables.

V.6 Terms of $O(\delta^2)$

For this order we will just apply the average operator to get a homogenized second correction. The $O(\delta^2)$ system is:

$$\begin{aligned}
 & (E^x E^y)^{-1} \sigma_{2,t}^x - (E^y)^{-1} P(\Sigma_0^x) (u_{2,x} + u_{3,\hat{x}}) \quad (\text{V.6.1a}) \\
 & - (E^y)^{-1} P'(\Sigma_0^x) \sigma_1^x (u_{1,x} + u_{2,\hat{x}}) - (E^y)^{-1} P'(\Sigma_0^x) \sigma_2^x (U_{0,x} + u_{1,\hat{x}}) \\
 & - \frac{1}{2} (E^y)^{-1} P''(\Sigma_0^x) (\sigma_1^x)^2 (U_{0,x} + u_{1,\hat{x}}) - (E^x)^{-1} Q(\Sigma_0^x) (v_{2,y} + \gamma^{-1} v_{3,\hat{y}}) \\
 & - (E^x)^{-1} Q'(\Sigma_0^x) \sigma_1^x (v_{1,y} + \gamma^{-1} v_{2,\hat{y}}) - (E^x)^{-1} Q'(\Sigma_0^x) \sigma_2^x (V_{0,y} + \gamma^{-1} v_{1,\hat{y}}) \\
 & \quad - \frac{1}{2} (E^x)^{-1} Q''(\Sigma_0^x) (\sigma_1^x)^2 (V_{0,y} + \gamma^{-1} v_{1,\hat{y}}) = 0,
 \end{aligned}$$

$$(E^x E^y)^{-1} \sigma_{2,t}^y - (E^x)^{-1} R(\Sigma_0^y) (v_{2,y} + \gamma^{-1} v_{3,\hat{y}}) \quad (\text{V.6.1b})$$

$$\begin{aligned} & - (E^x)^{-1} R'(\Sigma_0^y) \sigma_1^y (v_{1,y} + \gamma^{-1} v_{2,\hat{y}}) - (E^x)^{-1} R'(\Sigma_0^y) \sigma_2^y (V_{0,y} + \gamma^{-1} v_{1,\hat{y}}) \\ & - \frac{1}{2} (E^x)^{-1} R''(\Sigma_0^y) (\sigma_1^y)^2 (V_{0,y} + \gamma^{-1} v_{1,\hat{y}}) - (E^y)^{-1} S(\Sigma_0^y) (u_{2,x} + u_{3,\hat{x}}) \\ & - (E^y)^{-1} S'(\Sigma_0^y) \sigma_1^y (u_{1,x} + u_{2,\hat{x}}) - (E^y)^{-1} S'(\Sigma_0^y) \sigma_2^y (U_{0,x} + u_{1,\hat{x}}) \\ & - \frac{1}{2} (E^y)^{-1} S''(\Sigma_0^y) (\sigma_1^y)^2 (U_{0,x} + u_{1,\hat{x}}) = 0, \end{aligned}$$

$$\rho^x u_{2,t} - \sigma_{2,x}^x - \sigma_{3,\hat{x}}^x = 0, \quad (\text{V.6.1c})$$

$$\rho^y v_{2,t} - \sigma_{2,y}^y - \gamma^{-1} \sigma_{3,\hat{y}}^y = 0. \quad (\text{V.6.1d})$$

V.6.1 Averaged $O(\delta^2)$ system

Plug u_1 , v_1 , σ_1^x and σ_1^y from (V.4.3) respectively, u_2 , v_2 , σ_2^x and σ_2^y from (V.5.7), (V.5.3c) and (V.5.3d) respectively, the trivial solution for the first correction and use the homogenized leading order equations to express time derivatives in the leading order solutions as spatial derivatives into (V.6.1). In addition, apply the average operator. Doing so, we obtain:

$$E_h^x E_h^y \Sigma_{2,t}^x - E_h^y P(\Sigma_0^x) U_{2,x} - E_h^x Q(\Sigma_0^x) V_{2,y} \quad (\text{V.6.2a})$$

$$\begin{aligned} -E_h^y P'(\Sigma_0^x) \Sigma_2^x U_{0,x} - E_h^x Q'(\Sigma_0^x) \Sigma_2^x V_{0,y} &= \frac{E_h^y}{E_h^x} \mu_{11} P(\Sigma_0^x) U_{0,xxx} + \mu_{11} Q(\Sigma_0^x) V_{0,xxy} \\ &\quad + \frac{E_h^y}{E_h^x} \mu_{12} P'(\Sigma_0^x) \Sigma_{0,x}^x U_{0,xx} \\ &\quad + 2\mu_{11} Q'(\Sigma_0^x) \Sigma_{0,x}^x V_{0,xy} \\ &\quad + \frac{E_h^y}{2E_h^x} \mu_{12} P''(\Sigma_0^x) (\Sigma_{0,x}^x)^2 U_{0,x} \\ &\quad + \frac{1}{2} \mu_{12} Q''(\Sigma_0^x) (\Sigma_{0,x}^x)^2 V_{0,y} \\ &\quad + E_h^y \mu_{13} \Sigma_{0,x}^x [P'(\Sigma_0^x) \chi_2 + Q'(\Sigma_0^x) \chi_3], \end{aligned}$$

$$E_h^x E_h^y \Sigma_{2,t}^y - E_h^x R(\Sigma_0^y) V_{2,y} - E_h^y S(\Sigma_0^y) U_{2,x} \quad (\text{V.6.2b})$$

$$\begin{aligned} -E_h^x R'(\Sigma_0^y) \Sigma_2^y V_{0,y} - E_h^y S'(\Sigma_0^y) \Sigma_2^y U_{0,x} &= \frac{E_h^x}{E_h^y} \mu_{21} R(\Sigma_0^y) V_{0,yyy} + \mu_{21} S(\Sigma_0^y) U_{0,xyy} \\ &\quad + \frac{E_h^x}{E_h^y} \mu_{22} R'(\Sigma_0^y) \Sigma_{0,y}^y V_{0,yy} \\ &\quad + 2\mu_{21} S'(\Sigma_0^y) \Sigma_{0,y}^y U_{0,xy} \\ &\quad + \frac{E_h^x}{2E_h^y} \mu_{22} R''(\Sigma_0^y) (\Sigma_{0,y}^y)^2 V_{0,y} \\ &\quad + \frac{1}{2} \mu_{22} S''(\Sigma_0^y) (\Sigma_{0,y}^y)^2 U_{0,x} \\ &\quad + E_h^x \mu_{23} \Sigma_{0,y}^y [R'(\Sigma_0^y) \chi_4 + S'(\Sigma_0^y) \chi_1], \end{aligned}$$

$$\rho_h^x U_{2,t} - \Sigma_{2,x}^x = \frac{-\langle \rho^x F \rangle}{\rho_h^x} \Sigma_{0,xxx}^x + \mu_{31} \chi_{2,t}, \quad (\text{V.6.2c})$$

$$\rho_h^y V_{2,t} - \Sigma_{2,y}^y = \frac{-\langle \rho^y G \rangle}{\rho_h^y} \Sigma_{0,yyy}^y + \mu_{41} \chi_{4,t}, \quad (\text{V.6.2d})$$

where:

$$\begin{aligned}
\mu_{11} &= -\langle (E^x)^{-1} H \rangle, \\
\mu_{12} &= \langle (E^x)^{-1} C^2 \rangle - 2 \langle (E^x)^{-1} H \rangle, \\
\mu_{13} &= \langle (E^x)^{-1} C^2 \rangle, \\
\mu_{21} &= -\langle (E^y)^{-1} I \rangle, \\
\mu_{22} &= \langle (E^y)^{-1} D^2 \rangle - 2 \langle (E^y)^{-1} I \rangle, \\
\mu_{23} &= \langle (E^y)^{-1} D^2 \rangle, \\
\mu_{31} &= -\frac{(-1 + \alpha_x)^2 (\rho_1 - \rho_2)^2 [(-1 + \alpha_x) E_1 - \alpha_x E_2] \alpha_x^2}{12 E_1 E_2 [\alpha_x (\rho_1 - \rho_2) + \rho_2]}, \\
\mu_{41} &= -\gamma \frac{(-1 + \alpha_y)^2 (\rho_1 - \rho_2)^2 [(-1 + \alpha_y) E_1 - \alpha_y E_2] \alpha_y^2}{12 E_1 E_2 [\alpha_y (\rho_1 - \rho_2) + \rho_2]}.
\end{aligned}$$

V.7 Specific problem

Now that we have the homogenized leading order, first and second corrections, we will assume a specific form of the nonlinearity and work out the homogenized systems for this specific problem. We choose the constitutive relations to be as follows:

$$\sigma^x = \exp(aE^x\epsilon^x + bE^y\epsilon^y) - 1, \quad (\text{V.7.1a})$$

$$\sigma^y = \exp(cE^x\epsilon^x + dE^y\epsilon^y) - 1, \quad (\text{V.7.1b})$$

which implies:

$$P(\sigma^x) = a(\sigma^x + 1), \quad (\text{V.7.2a})$$

$$Q(\sigma^x) = b(\sigma^x + 1), \quad (\text{V.7.2b})$$

$$R(\sigma^y) = d(\sigma^y + 1), \quad (\text{V.7.2c})$$

$$S(\sigma^y) = c(\sigma^y + 1). \quad (\text{V.7.2d})$$

Considering (V.7.2), the homogenized leading order (V.4.2) becomes:

$$E_h^x E_h^y \Sigma_{0,t}^x - a E_h^y (\Sigma_0^x + 1) U_{0,x} - b E_h^x (\Sigma_0^x + 1) V_{0,y} = 0, \quad (\text{V.7.3a})$$

$$E_h^x E_h^y \Sigma_{0,t}^y - d E_h^x (\Sigma_0^y + 1) V_{0,y} - c E_h^y (\Sigma_0^y + 1) U_{0,x} = 0, \quad (\text{V.7.3b})$$

$$\rho_h^x U_{0,t} - \Sigma_{0,x}^x = 0, \quad (\text{V.7.3c})$$

$$\rho_h^y V_{0,t} - \Sigma_{0,y}^y = 0. \quad (\text{V.7.3d})$$

Since the solution of the homogenized first correction vanishes, we don't consider it here. Plugging (V.7.1) and (V.7.2) into the homogenized second correction (V.6.2), we get:

$$\begin{aligned} E_h^x E_h^y \Sigma_{2,t}^x - a E_h^y (\Sigma_0^x + 1) U_{2,x} - b E_h^x (\Sigma_0^x + 1) V_{2,y} \\ - a E_h^y \Sigma_2^x U_{0,x} - b E_h^x \Sigma_2^x V_{0,y} = a \frac{E_h^y}{E_h^x} \mu_{11} (\Sigma_0^x + 1) U_{0,xxx} \\ + b \mu_{11} (\Sigma_0^x + 1) V_{0,xxy} \\ + \mu_{12} \Sigma_{0,x}^x \left(a \frac{E_h^y}{E_h^x} U_{0,xx} + b V_{0,xy} \right), \end{aligned} \quad (\text{V.7.4a})$$

$$E_h^x E_h^y \Sigma_{2,t}^y - d E_h^x (\Sigma_0^y + 1) V_{2,y} - c E_h^y (\Sigma_0^y + 1) U_{2,x} \quad (\text{V.7.4b})$$

$$\begin{aligned} -d E_h^x \Sigma_2^y V_{0,y} - c E_h^y \Sigma_2^y U_{0,x} &= d \frac{E_h^x}{E_h^y} \mu_{21} (\Sigma_0^y + 1) V_{0,yyy} \\ &\quad + c \mu_{21} (\Sigma_0^y + 1) U_{0,xyy} \\ &\quad + \mu_{22} \Sigma_{0,y}^y \left(d \frac{E_h^x}{E_h^y} V_{0,yy} + c U_{0,xy} \right), \end{aligned}$$

$$\rho_h^x U_{2,t} - \Sigma_{2,x}^x = \mu_{32} \Sigma_{0,xxx}^x + \mu_{33} \Sigma_{0,xyy}^y, \quad (\text{V.7.4c})$$

$$\rho_h^y V_{2,t} - \Sigma_{2,y}^y = \mu_{42} \Sigma_{0,yyy}^y + \mu_{43} \Sigma_{0,xyy}^x, \quad (\text{V.7.4d})$$

where:

$$\begin{aligned} \mu_{32} &= -\frac{\langle \rho^x F \rangle}{\rho_h^x} + \frac{bc}{ad - bc} (E_h^x \rho_h^x)^{-1} \mu_{31}, \\ \mu_{33} &= \frac{bd}{ad - bc} (E_h^y \rho_h^y)^{-1} \mu_{31}, \\ \mu_{42} &= -\frac{\langle \rho^y G \rangle}{\rho_h^y} + \frac{bc}{ad - bc} (E_h^y \rho_h^y)^{-1} \mu_{41}, \\ \mu_{43} &= \frac{ac}{ad - bc} (E_h^x \rho_h^x)^{-1} \mu_{41}. \end{aligned}$$

V.7.1 Combining the homogenized systems

To get a final system, we need to combine the homogenized leading order along with the homogenized corrections. To do this we use the original expansion (V.2.2) and apply the double average operator:

$$\langle u \rangle = u = U_0 + \delta^2 U_2 + O(\delta^3), \quad (\text{V.7.5a})$$

$$\langle v \rangle = v = V_0 + \delta^2 V_2 + O(\delta^3), \quad (\text{V.7.5b})$$

$$\langle \sigma^x \rangle = \sigma^x = \Sigma_0^x + \delta^2 \Sigma_2^x + O(\delta^3), \quad (\text{V.7.5c})$$

$$\langle \sigma^y \rangle = \sigma^y = \Sigma_0^y + \delta^2 \Sigma_2^y + O(\delta^3), \quad (\text{V.7.5d})$$

where we no longer use the convention that upper case for the solution variables denotes independence of the fast scales. This is because the next step will bring the final system for which we want to keep the notation as simple and clear as possible.

Considering (V.7.5) we add up the systems (V.7.3) and (V.7.4) to obtain:

$$E_h^x E_h^y \sigma_t^x - a E_h^y (\sigma^x + 1) u_x \quad (\text{V.7.6a})$$

$$\begin{aligned} -b E_h^x (\sigma^x + 1) v_y &= \delta^2 \mu_{11} (\sigma^x + 1) \left(a \frac{E_h^y}{E_h^x} u_{xxx} + b v_{xxy} \right) \\ &\quad + \delta^2 \mu_{12} \sigma_x^x \left(a \frac{E_h^y}{E_h^x} u_{xx} + b v_{xy} \right) + O(\delta^3), \end{aligned}$$

$$E_h^x E_h^y \sigma_t^y - d E_h^x (\sigma^y + 1) v_y \quad (\text{V.7.6b})$$

$$\begin{aligned} -c E_h^y (\sigma^y + 1) u_x &= \delta^2 \mu_{21} (\sigma^y + 1) \left(d \frac{E_h^x}{E_h^y} v_{yyy} + c u_{xyy} \right) \\ &\quad + \delta^2 \mu_{22} \sigma_y^y \left(d \frac{E_h^x}{E_h^y} v_{yy} + c u_{xy} \right) + O(\delta^3), \end{aligned}$$

$$\rho_h^x u_t - \sigma_x^x = \delta^2 \mu_{32} \sigma_{xxx}^x + \delta^2 \mu_{33} \sigma_{xxy}^y, \quad (\text{V.7.6c})$$

$$\rho_h^y v_t - \sigma_y^y = \delta^2 \mu_{42} \sigma_{yyy}^y + \delta^2 \mu_{43} \sigma_{xxy}^x. \quad (\text{V.7.6d})$$

As mentioned, this is the final system we consider in this section. One can notice the left hand side has the same form as the original variable coefficient system (V.1.6) but with average constant coefficients.

Chapter VI

Numerical solution of the homogenized system

In this chapter, we find the numerical solution of the homogenized system (V.7.6) and compare it with the solution of (IV.6.2) through finite volumes.

For simplicity, we express the homogenized system (V.7.6) in the following way:

$$q_t = g(q, q_x, q_{xx}, q_{xxx}, q_y, q_{yy}, q_{yyy}, q_{xyy}, q_{xxy}), \quad (\text{VI.0.1})$$

where $q = \begin{bmatrix} \sigma^x & \sigma^y & u & v \end{bmatrix}^T$ is the solution vector and $g(q, \dots)$ are all the terms involving the solution and its spatial derivatives.

VI.1 Spatial discretization

We use pseudospectral discretization in space. This has several advantages such as low storage, low computational cost due to the use of Fast Fourier Transform (FFT), spectral accuracy, easy to deal with nonlinearities and others. The input for the spatial discretization is the current value of the solution and the output is the discretized right hand side of (VI.0.1), which we denote as $G(Q)$, where Q is a

discretized version of q . Applying the spatial discretization, we get:

$$Q_t = G(Q). \quad (\text{VI.1.1})$$

One can refer to [24, 25] for details about pseudospectral methods.

VI.2 Time integration

Since (VI.1.1) is a stiff system, an implicit A-stable method is convenient; thus, we use backward Euler integration in time. Applying backward Euler to (VI.1.1) yields:

$$F(q^{n+1}) \equiv q^{n+1} - \Delta t G(q^{n+1}) - q^n = 0, \quad (\text{VI.2.1})$$

where Δt is the size of the time step. Equation (VI.2.1) is a nonlinear system of equations that has to be solved at each time step. One can solve it by Newton's method. Doing so, we get the following iteration formula:

$$q_{k+1}^{n+1} = q_k^n + d_k,$$

where k is an index for the Newton's iteration and d_k is given by:

$$J(q_k^{n+1}) d_k = -F(q_k^{n+1}), \quad (\text{VI.2.2})$$

where $J(q_k^{n+1})$ is the Jacobian matrix of $F(q_k^{n+1})$. The Jacobian may be found exactly or approximated by finite differences. In either case, it is large enough to create memory storage issues. As a consequence, we use a Jacobian-free approach based on approximating the multiplication of the Jacobian times a vector by Taylor series. First and second order approximations of $J(q)d$ are [26]:

$$\begin{aligned} J(q)d &\approx \frac{F(q + \epsilon d) - F(q)}{\epsilon}, \\ J(q)d &\approx \frac{F(q + \epsilon d) - F(q - \epsilon d)}{\epsilon}. \end{aligned}$$

where ϵ is a small parameter. Several options are available for ϵ in [26].

Once we have the approximation of $J(q_k^{n+1})d_k$ we have to solve the linear system (VI.2.2). Since we don't have the Jacobian explicitly, we must apply a matrix-free method to solve linear systems. A convenient choice is to use an iterative method based on Krylov subspaces such as GMRES or CG. In this work we use GMRES.

The generalized minimal residuals or GMRES is a method to solve iteratively the linear problem $Ax = b$. This method can be viewed as the least squares problem that minimizes the residual:

$$\min \|r_n\| = \min \|b - Ax_n\|,$$

where x_n belongs to the Krylov subspace of A , which is given by $\langle b, Ab, \dots, A^{n-1}b \rangle$. To do this, we just require knowing the action of A on any vector. One may refer to [27] for details.

Finally, we are able to solve the linear system (VI.2.2) until we converge to the nonlinear solution of (VI.2.1). We have to repeat this at each time step until we reach the final desired time.

VI.3 Linear case

Figure VI.3.1 shows the numerical solution of (V.7.6) using the mentioned approach. In addition, we compare the solution of the variable coefficient system (IV.6.2) using finite volume methods implemented in Clawpack. The material parameters are:

$$E_1 = \rho_1 = 1, \quad (\text{VI.3.1a})$$

$$E_2 = \rho_2 = 2, \quad (\text{VI.3.1b})$$

and the constitutive relations are:

$$\begin{aligned} \sigma^x &= E^x \epsilon^x + 0.75 E^y \epsilon^y, \\ \sigma^y &= 0.75 E^x \epsilon^x + E^y \epsilon^y, \end{aligned}$$

where E^x and E^y are periodic piecewise constant functions that vary just in x and y respectively and are defined by E_1 and E_2 . The length of the period is set to unity and E_1 and E_2 are equally distributed within a period; the same is true for ρ^x and ρ^y in (IV.6.2). For the finite volume simulation we use 2000 grid cells per direction while we consider just 256 grid cells per direction for the numerical solution of the homogenized system.

VI.4 Nonlinear case

In figure VI.4.1, we compare the nonlinear version of (V.7.6) using the mentioned numerical approach and (IV.6.2) using finite volumes. The material parameters are the same as in the linear case (VI.3.1) while the constitutive relations are given by:

$$\begin{aligned} \sigma^x &= \exp(E^x \epsilon^x + 0.75 E^y \epsilon^y), \\ \sigma^y &= \exp(0.75 E^x \epsilon^x + E^y \epsilon^y). \end{aligned}$$

We can observe a good match in both the linear and the nonlinear case up to the computed time. In figure VI.4.2, we can see a close-up of the solution at time $t = 5$. Note that the solution of the homogenized equations is smoother. This is expectable since during the homogenization process we average information regarding the fast spatial variables. As a result, we just obtain the effect of those variations in the macroscopic level. One can also notice from this figure the difference in the number of grid points used. For the solution of the variable coefficient system through finite volumes we must consider a finer grid to resolve properly the solution, in this case 2000 grid cells are being used in each direction. On the other hand, to solve the homogenized equations one can use coarser grids, in this case, where we use pseudospectral discretization in space, 256 grid cells are used in each direction.

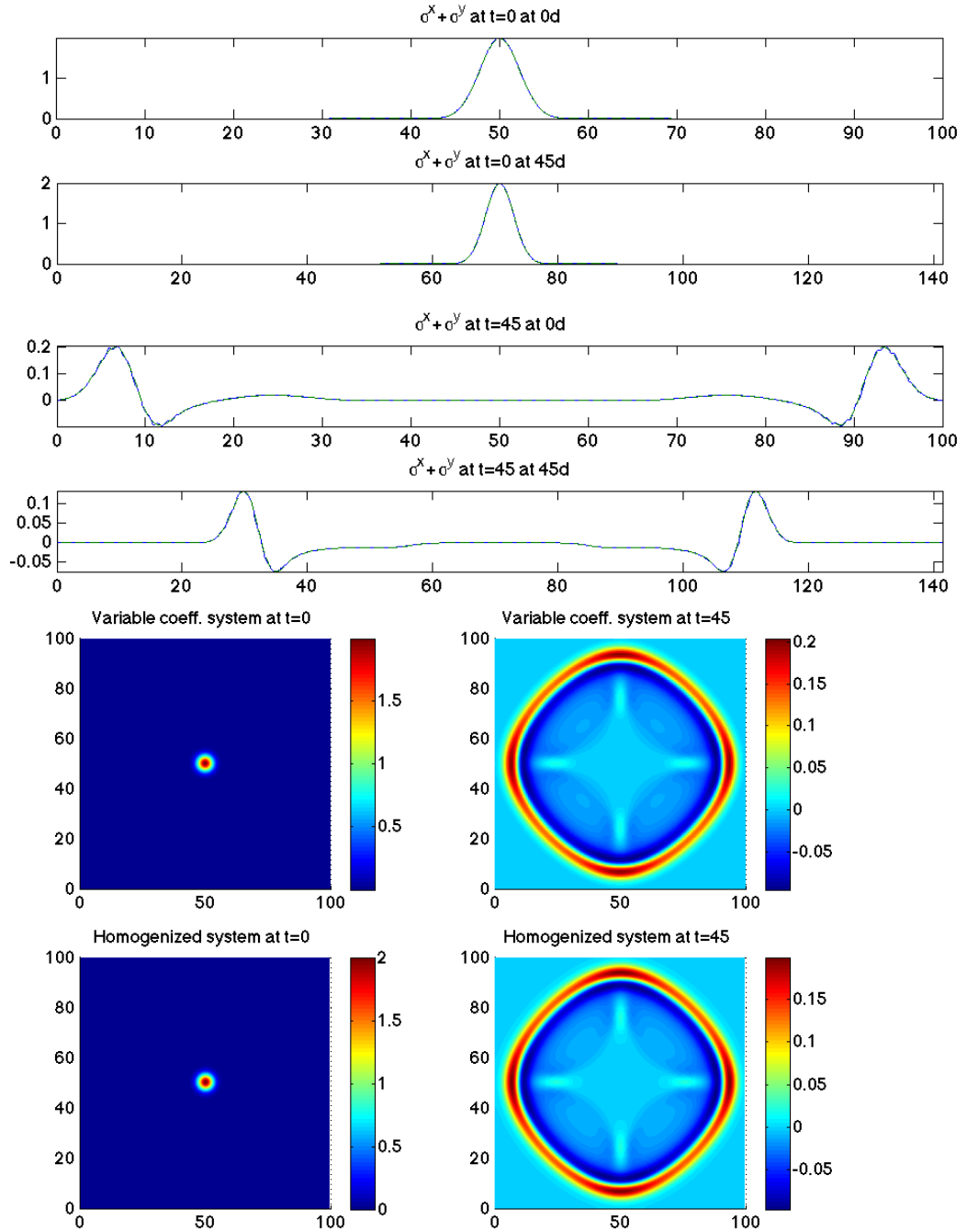


Figure VI.3.1: Comparison between the variable coefficient system (IV.6.2) and homogenized system (V.7.6) for the linear case. At the top 1D plots of slices are shown at 0° and 45° with respect to the center of the domain. The solid line corresponds to the variable coefficient system while the dashed line to the homogenized equations. At the bottom, the corresponding 2D surface plots.

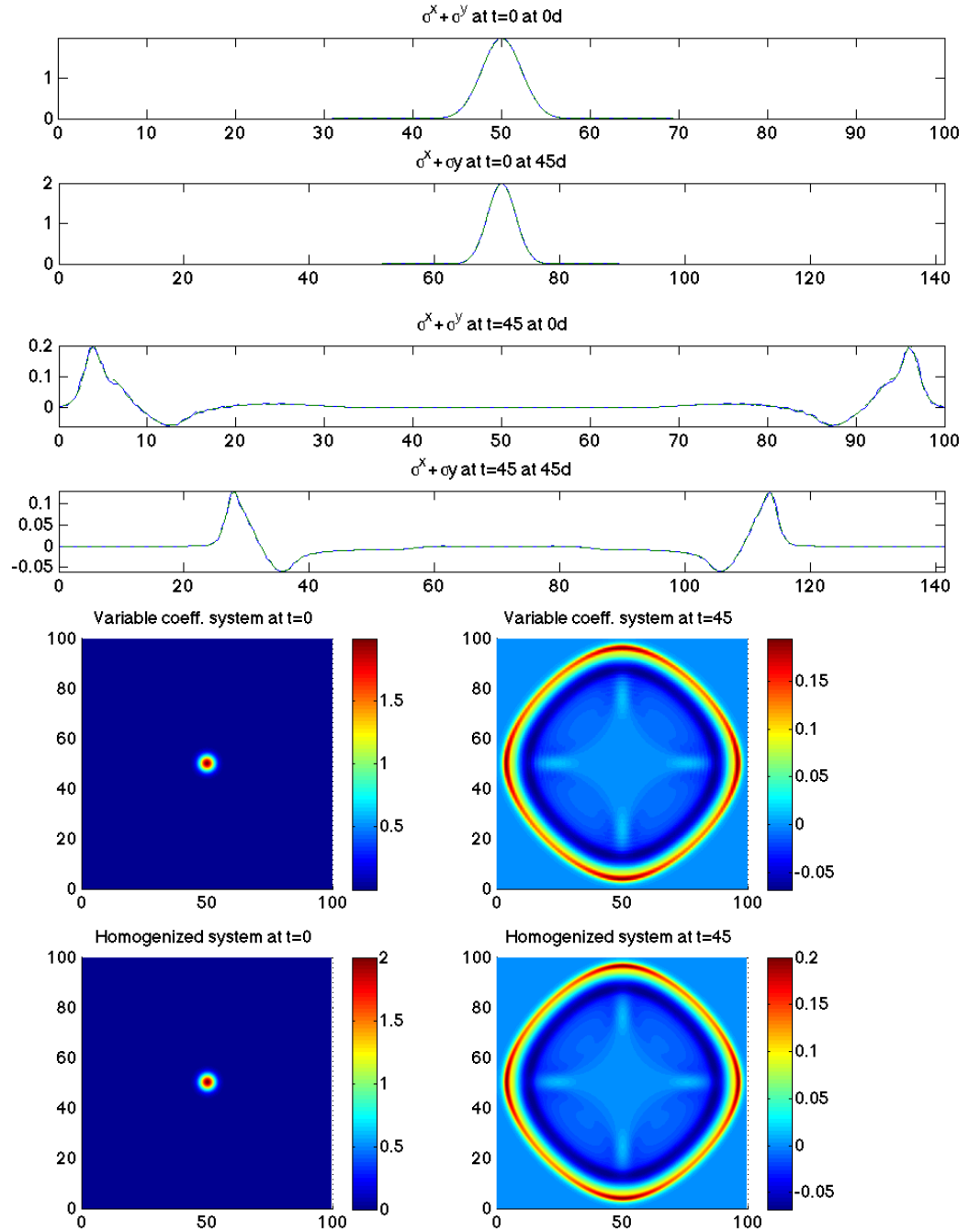


Figure VI.4.1: Comparison between the variable coefficient system (IV.6.2) and homogenized system (V.7.6) for the nonlinear case. At the top 1D plots of slices are shown at 0° and 45° with respect to the center of the domain. The solid line corresponds to the variable coefficient system while the dashed line to the homogenized equations. At the bottom, the corresponding 2D surface plots.

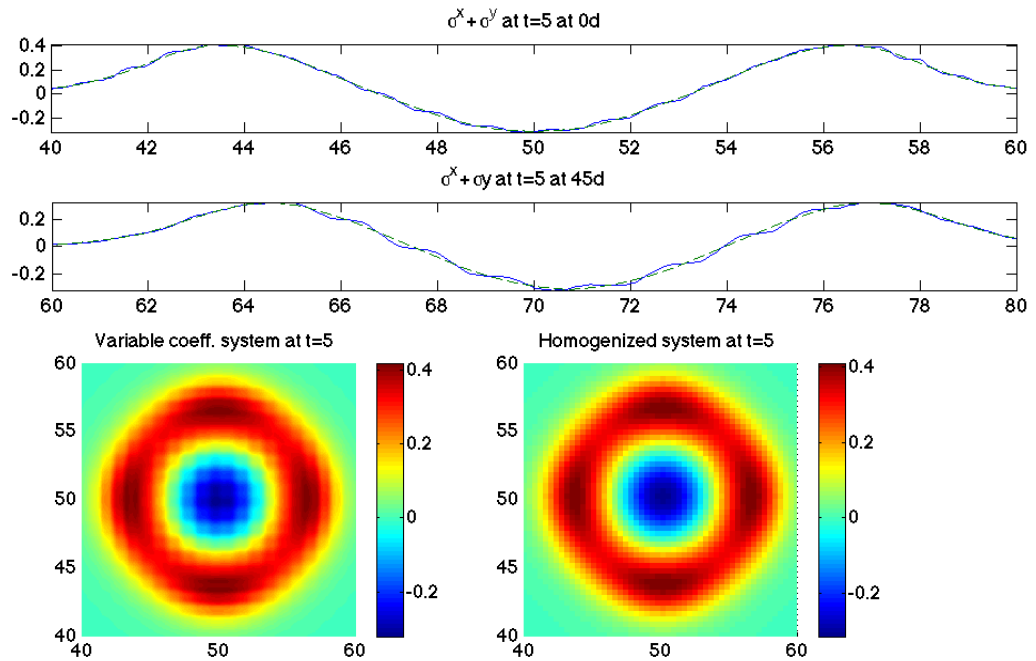


Figure VI.4.2: Comparison between the variable coefficient system (IV.6.2) and homogenized system (V.7.6) for the nonlinear case. At the top 1D plots of slices are shown at 0° and 45° with respect to the center of the domain. The solid line corresponds to the variable coefficient system while the dashed line to the homogenized equations. At the bottom, the corresponding 2D surface plots.

Chapter VII

About the stability of the homogenized system

In the previous chapter, we got the solution of the homogenized equation up to time $t = 45$ and obtained a good agreement with the finite volume solution of the original variable coefficient system for the particular set of chosen parameters. Nevertheless, the system doesn't behave stable in general. Considering:

$$E_1 = \rho_1 = 1,$$

$$E_2 = \rho_2 = 10,$$

we obtain the numerical solution of the homogenized equations (V.7.6) and get the results in figure VII.0.1. The corresponding simulation of the variable coefficient system (IV.6.2) using finite volumes is also shown as reference in such figure. It is evident a stability issue is present in the numerical solution of the homogenized equations after certain time. Recall we implement an A-stable implicit time integrator, which implies the numerical solution is stable as long as all eigenvalues lie within the left half part of the complex plane. Therefore, we must have some positive real eigenval-

ues. In figure VII.0.2 we plot the eigenvalues of the linear version of $G(Q)$ in (VI.1.1) considering just 32 grid points in each direction. We observe indeed the presence of some positive and real eigenvalues. Having positive real eigenvalues implies the homogenized system is unstable by itself.

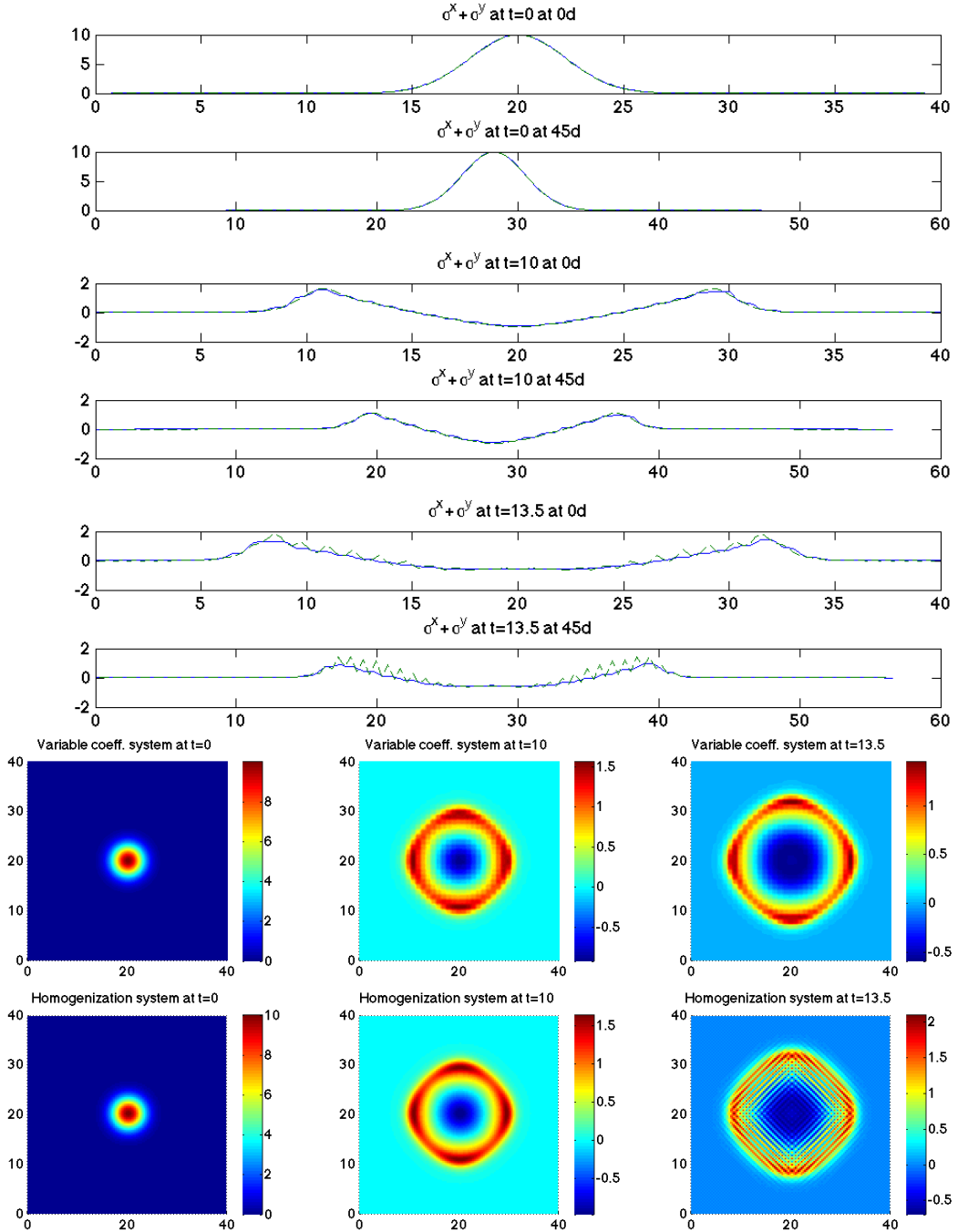


Figure VII.0.1: Comparison between the homogenized system (V.7.6) and the variable coefficient system (IV.6.2) for the nonlinear case. At the top 1D plots of slices are shown at 0° and 45° with respect to the center of the domain. The solid line corresponds to the variable coefficient system while the dashed line to the homogenized equations. At the bottom, the corresponding 2D surface plots.

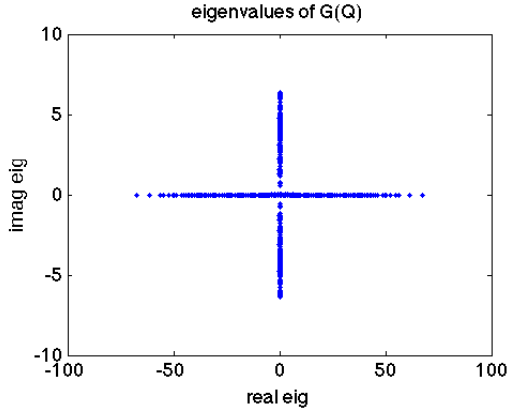


Figure VII.0.2: Eigenvalues of $G(Q)$ in (VI.1.1). Real positive eigenvalues are present making the system unstable.

VII.1 Stability of 1D homogenized system

To understand the stability properties of the homogenized equations (V.7.6), we study a 1D linear version of them, which is given by:

$$\sigma_t = E_h^{-1}u_x + \delta^2 E_h^{-2}\mu_{11}u_{xxx}, \quad (\text{VII.1.1a})$$

$$u_t = \rho_h^{-1}\sigma_x + \delta^2 \rho_h^{-1}\mu_{21}\sigma_{xxx}, \quad (\text{VII.1.1b})$$

where the coefficients become:

$$\mu_{11} = -\langle E^{-1}H \rangle,$$

$$\mu_{21} = -\frac{\langle \rho F \rangle}{\rho_h}.$$

Note that since this is a 1D situation we drop the superscript to denote either the x or y component of all functions. System (VII.1.1) can be written as:

$$\bar{q}_t + \mathbf{A}\bar{q}_x + \mathbf{B}\bar{q}_{xxx} = \bar{0}, \quad (\text{VII.1.2})$$

where:

$$\begin{aligned}\bar{q} &= \begin{bmatrix} \sigma \\ u \end{bmatrix}, \\ \mathbf{A} &= \begin{bmatrix} 0 & -E_h^{-1} \\ -\rho_h^{-1} & 0 \end{bmatrix}, \\ \mathbf{B} &= \begin{bmatrix} 0 & -\delta^2 E_h^{-2} \mu_{11} \\ -\delta^2 \rho_h^{-1} \mu_{21} & 0 \end{bmatrix},\end{aligned}$$

One may study the stability of the system by assuming:

$$\bar{q}(x, t) = \hat{q}(t) \exp(ikx). \quad (\text{VII.1.3})$$

Plugging (VII.1.3) into (VII.1.2), we obtain:

$$\hat{q}(t) = \hat{q}(0) \exp[-ik(\mathbf{A} - k^2 \mathbf{B})t].$$

The eigenvalues of $\mathbf{A} - k^2 \mathbf{B}$ determine the behavior of the system. Each eigenmode may have a different behavior. Having eigenvalues:

- purely real, make the associated mode be purely oscillatory and hence stable.
- negative and imaginary, make the corresponding mode decay exponentially.
- positive and imaginary, make the corresponding mode grow exponentially and, therefore, cause the whole solution to be unstable.

The mentioned eigenvalues are:

$$\begin{aligned}\lambda_1 &= -\frac{\sqrt{-(E_h - k^2 \mu_{11})(-1 + k^2 \mu_{21})}}{E_h \sqrt{\rho_h}}, \\ \lambda_2 &= \frac{\sqrt{-(E_h - k^2 \mu_{11})(-1 + k^2 \mu_{21})}}{E_h \sqrt{\rho_h}}.\end{aligned}$$

The nature of the eigenvalues depends completely on the coefficients μ_{11} and μ_{21} , which are determined by the material properties. By choosing:

$$E_1 = \rho_1 = 4, \quad (\text{VII.1.5a})$$

$$E_2 = \rho_2 = 1, \quad (\text{VII.1.5b})$$

we get:

$$\begin{aligned}\lambda_1 &= -\frac{4}{5} \left(1 - \frac{3k^2}{200}\right), \\ \lambda_2 &= \frac{4}{5} \left(1 - \frac{3k^2}{200}\right).\end{aligned}$$

We can see that the eigenvalues are purely real and, as a result, the solution is purely oscillatory; hence, stable. This, however, is not always true. If, for instance, we let:

$$E_1 = \rho_1 = 4, \quad (\text{VII.1.6a})$$

$$E_2 = 1, \quad (\text{VII.1.6b})$$

$$\rho_2 = 4, \quad (\text{VII.1.6c})$$

then the eigenvalues are given by:

$$\begin{aligned}\lambda_1 &= -\frac{4}{5}\sqrt{\frac{5}{8} - \frac{3k^2}{640}}, \\ \lambda_2 &= \frac{4}{5}\sqrt{\frac{5}{8} - \frac{3k^2}{640}},\end{aligned}$$

from which is evident the presence of positive and negative imaginary eigenvalues for some values of k leading to an unstable solution.

In figure VII.1.1, we show the solution of the homogenized system in 1D from (VII.1.2) corresponding to the parameters (VII.1.5) and (VII.1.6). As expected, the solution becomes unstable for the second set of parameters.

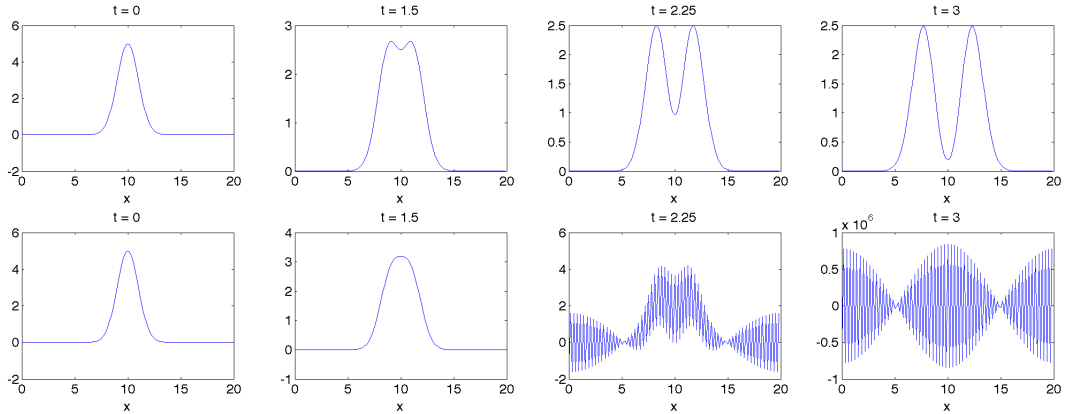


Figure VII.1.1: Stable (top) and unstable (bottom) 1D linear homogenized system (VII.1.2) using (VII.1.5) and (VII.1.6) respectively.

VII.2 Another unstable 1D homogenized system

As mentioned in Chapter II, there are several approaches to get homogenized equations. In [5] a different approach is considered for the same 1D p-system considered in the previous section. Moreover, this homogenized system is considered in the context of stegoton formation. A linear version of such system is:

$$\bar{q}_t + \mathbf{D}\bar{q}_x + \mathbf{E}\bar{q}_{xxx} = \bar{0}, \quad (\text{VII.2.1})$$

where:

$$\begin{aligned}\bar{q} &= \begin{bmatrix} \sigma \\ u \end{bmatrix}, \\ \mathbf{D} &= \begin{bmatrix} 0 & -\langle E^{-1} \rangle^{-1} \\ -\langle \rho \rangle^{-1} & 0 \end{bmatrix}, \\ \mathbf{E} &= \begin{bmatrix} 0 & \delta^2 \langle E^{-1} \rangle^{-1} C_{12} \\ \delta^2 \langle \rho \rangle^{-1} C_{22} & 0 \end{bmatrix},\end{aligned}$$

where:

$$\begin{aligned}C_{12} &= -\frac{1}{12} \alpha^2 (1-\alpha)^2 \frac{(\rho_1 - \rho_2)(\rho_1 E_1 - \rho_2 E_2)}{E_1 E_2 \langle E^{-1} \rangle \langle \rho \rangle^2}, \\ C_{22} &= -\frac{1}{12} \alpha^2 (1-\alpha)^2 \frac{(E_1 - E_2)(\rho_1 E_1 - \rho_2 E_2)}{E_1^2 E_2^2 \langle E^{-1} \rangle^2 \langle \rho \rangle}.\end{aligned}$$

As in the previous section, one can show (VII.2.1) is not stable in general. In figure VII.2.1, we show the solution corresponding to the parameters (VII.1.5) and (VII.1.6). Again, the solution becomes unstable for the second set of parameters.

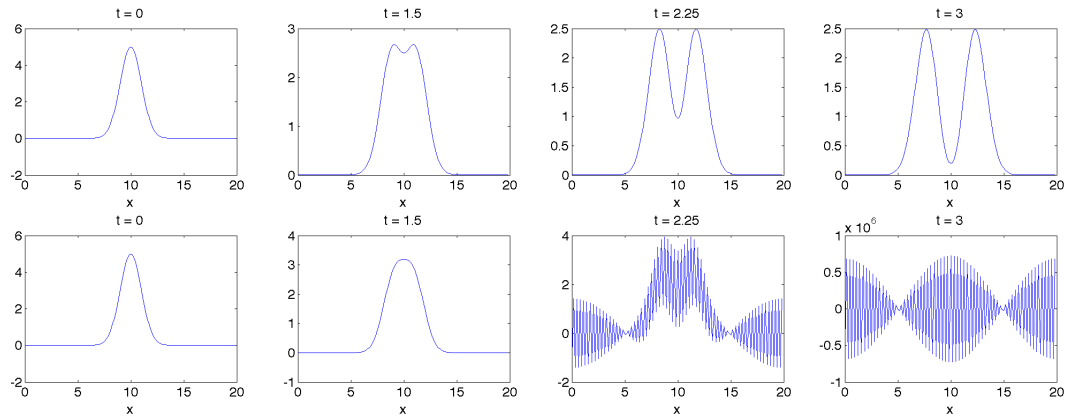


Figure VII.2.1: Stable (top) and unstable (bottom) 1D linear homogenized system (VII.2.1) using (VII.1.5) and (VII.1.6) respectively.

Conclusions and future directions

Regarding stegoton formation in 2D, we found solitary wave formation does happen in the propagation of nonlinear waves in heterogeneous media extending the results in [5] to the 2D case. We observed the importance of numerical dissipation in 2D solitary wave formation and how it may prevent the stegoton formation. We saw the solitary waves may occur in a single direction if the material is heterogeneous just in that direction while a shock happens in the homogeneous direction. In the context of long thin domains, we observed having a more homogeneous material in the transverse direction enhances solitary wave formation.

With respect to the homogenized equations, they are stiff enough so that an implicit A-stable integration in time is worthwhile. Jacobian-free Newton Krylov methods are convenient for the solution of the nonlinear equation arising from the implicit time integration since the required Jacobian in conventional methods is too large to store.

A good agreement between the homogenized equations and the variable coefficient system is observed when the homogenized system is stable. Nevertheless, the homogenized system is not stable in general. Studying the 1D version of it by two different homogenization approaches we found neither is stable in general. The variable coefficient system is stable for any choice of the material parameters (assuming they are all positive). Therefore, the instability is being created by the homogenization and is present in the two approaches considered.

Future directions

Future research directions with respect to 2D stegotons are to implement a higher order scheme and consider behavior at longer times, interaction of 2D stegotons, different kind of non-homogeneous domains and others.

Future directions regarding the homogenization are to study the source and nature of the instability. It is important to understand why this is happening and how it may be avoided to find effective equations stable in every situation.

BIBLIOGRAPHY

- [1] N. Zabusky and M. Kruskal, "Interaction of" solitons" in a collisionless plasma and the recurrence of initial states," *Physical Review Letters*, vol. 15, no. 6, pp. 240–243, 1965.
- [2] F. Santosa and W. Symes, "A dispersive effective medium for wave propagation in periodic composites," *SIAM Journal on Applied Mathematics*, vol. 51, no. 4, pp. 984–1005, 1991.
- [3] J. Fish and W. Chen, "Higher-order homogenization of initial/boundary-value problem," *Journal of Engineering Mechanics*, vol. 127, no. 12, pp. 1223–1230, 2001.
- [4] W. Chen and J. ASME, "A dispersive model for wave propagation in periodic heterogeneous media based on homogenization with multiple spatial and temporal scales," *Journal of Applied Mechanics*, vol. 68, p. 153, 2001.
- [5] R. Leveque and D. Yong, "Solitary waves in layered nonlinear media," *SIAM Journal on Applied Mathematics*, vol. 63, no. 5, pp. 1539–1560, 2003.
- [6] R. J. LeVeque and M. J. Berger, "Clawpack software version 4.5," 2011. Url: www.clawpack.org.
- [7] A. Alghamdi, A. Ahmadia, D. Ketcheson, M. Knepley, K. Mandli, and L. Dalcin, *PetClaw: A Scalable Parallel Nonlinear Wave Propagation Solver*

- for Python.* ACM, 2011. To appear in proceedings of HPC 2011. Url: <http://web.kaust.edu.sa/faculty/davidketcheson/petclaw.pdf>.
- [8] S. Balay, K. Buschelman, V. Eijkhout, W. Gropp, D. Kaushik, M. Knepley, L. McInnes, B. Smith, and H. Zhang, “PETSc Web page,” 2010.
 - [9] R. LeVeque, *Finite volume methods for hyperbolic problems*. Cambridge Univ Pr, 2002.
 - [10] R. LeVeque, “Wave propagation algorithms for multidimensional hyperbolic systems* 1,” *Journal of Computational Physics*, vol. 131, no. 2, pp. 327–353, 1997.
 - [11] D. Bale, R. LeVeque, S. Mitran, and J. Rossmanith, “A wave propagation method for conservation laws and balance laws with spatially varying flux functions,” *SIAM Journal on Scientific Computing*, vol. 24, no. 3, pp. 955–978, 2003.
 - [12] G. Pavliotis and A. Stuart, *Multiscale methods: averaging and homogenization*. Springer Verlag, 2008.
 - [13] A. Bensoussan, J. Lions, and G. Papanicolaou, *Asymptotic analysis for periodic structures*. North Holland, 1978.
 - [14] J. Kevorkian and J. Cole, *Multiple scale and singular perturbation methods*. Springer Verlag, 1996.
 - [15] E. Hinch, *Perturbation methods*. Cambridge Univ Pr, 1991.
 - [16] J. Kevorkian and D. Bosley, “Multiple-scale homogenization for weakly nonlinear conservation laws with rapid spatial fluctuations,” *Studies in Applied Mathematics*, vol. 101, no. 2, pp. 127–183, 1998.
 - [17] J. Auriault, “Heterogeneous medium. Is an equivalent macroscopic description possible?,” *International journal of engineering science*, vol. 29, no. 7, pp. 785–795, 1991.

- [18] N. Wellander and G. Kristensson, “Homogenization of the Maxwell equations at fixed frequency,” *SIAM Journal on Applied Mathematics*, vol. 64, no. 1, pp. 170–195, 2003.
- [19] H. Banks, V. Bokil, D. Cioranescu, N. Gibson, G. Griso, and B. Miara, “Homogenization of periodically varying coefficients in electromagnetic materials,” *Journal of Scientific Computing*, vol. 28, no. 2, pp. 191–221, 2006.
- [20] L. Barker, “A model for stress wave propagation in composite materials,” *Journal of Composite Materials*, vol. 5, no. 2, p. 140, 1971.
- [21] R. LeVeque, “Finite-volume methods for non-linear elasticity in heterogeneous media,” *International Journal for Numerical Methods in Fluids*, vol. 40, no. 1-2, pp. 93–104, 2002.
- [22] D. Ketcheson, *High Order Strong Stability Preserving Time Integrators and Numerical Wave Propagation Methods for Hyperbolic PDEs*. PhD thesis, Citeseer, 2009.
- [23] R. LeVeque, *Finite difference methods for ordinary and partial differential equations*. Society for Industrial and Applied Mathematics, 2007.
- [24] L. Trefethen, *Spectral methods in MATLAB*. Society for Industrial Mathematics, 2000.
- [25] B. Fornberg, *A practical guide to pseudospectral methods*. Cambridge Univ Pr, 1998.
- [26] D. Knoll and D. Keyes, “Jacobian-free Newton-Krylov methods: a survey of approaches and applications,” *Journal of Computational Physics*, vol. 193, no. 2, pp. 357–397, 2004.

- [27] L. Trefethen and D. Bau, *Numerical linear algebra*. Society for Industrial Mathematics, 1997.